Dear Editor,

We thank the reviewers for careful and critical reading of the manuscript and triggering a large and useful number of improvements. The revised version contains a large number of new aspects and changes. Because of the many changes and to keep the text readable, we found it inappropriate to mark all these changes in the revised version.

Before we answer all the questions and comments of the reviewers (step by step), we would like to give an overview of all major changes, right in the beginning.

1) We changed and simplified the notation throughout the paper significantly, to come close to a more general notation (common in the used CCN and INP-related literature): n_{CCN}, n_{INP}, n_{50}, n_{250} etc, only! … in the equations and in the text. No longer APC, ASC, INPC…. .

2) We switched from ***ambient*** particle number and surface area concentrations n_{50}, n_{250}, s, … to ***dry particle*** number and surface area concentrations $n_{50,dry}$, $n_{250,dry}$, s_{dry} in our correlation study and CCN and INP retrieval schemes. That means we include the particle water-uptake effect (and required corrections) in our methodology. Water up-take effects are different for desert dust, continental aerosol mixtures, and marine particles. We discuss this in Sect. 3.2.

3) As a consequence of the consideration of particle water uptake effects, the correlated parameters in the AERONET data analysis (Figs. 4,5, and 7 in Sect 4.1-4.2) changed, and all conversion factors obtained from the correlation analysis changed in Table 3 (except for hydrophobic dust).

4) Different CCN retrieval schemes (Sect. 3.2) are now used for hydrophobic desert dust particles and for hygroscopic aerosol components (continental, marine). Because of the hydrophobic nature of dust the critical CCN-related dust particle diameter is a factor of 2 larger (critical activation radius is about100 nm for supersaturations of 0.2%) as in the case of hygroscopic particles (critical activation radius is about 50 nm for a supersaturation of 0.2%). This is now discussed in Sect. 1 and 3.3 and considered in CCN parameterization.

5) We included a new topic: INP parameterization for marine particles (in Sect. 3.4.1)! We use the latest study on the INP efficacy of marine particles of DeMott et al., 2015 (PNAS paper, early edition, Dec. 2015). The INP efficacy of marine particles (sea salt) is about a factor of 300-500 lower than for terrestrial particles.

6) We provide an extended discussion why we use the DeMott (2010) INP parameterization for non-desert continental aerosols (see Sect. 3.4.1).

7) We extensively compare our correlation results (n_{CCN} from particle extinction coefficients) with findings of Shinozuka et al. (2015) and Sakai et al. (2013) in Sect.4.1, 4.2, and 4.3. We even show n_{CCN} profiles after Shinozuka et al. (2015) for comparison with the lidar-derived profiles in Sect.5.1 and 5.2 (lidar case studies).

8) We improved Table 3, and now provide uncertainties for all conversion parameters.

9) We introduced a new Table 4 to provide an overview of typical uncertainties in all the retrieval products (optical, microphysical, and the cloud-relevant aerosol properties).

10) We finally substituted all Leipzig AERONET results (based on AERONET level-1.5 data) by level 2.0-data which became available in December 2015.

11) We use the AERONET uncertainty study of Dubovik et al. (2000) to provide a better error discussion of the basic AERONET aerosol products (size distribution, number concentration, surface area concentration) in Sect. 2.1.

12) Because of all necessary changes many new references (about 20) are included in the revised manuscript.

Step-by-step answers:

Reviewer #1:

I have only one minor comment regarding the Figure 5, middle: it seems that something is wrong with the regression line for the green dots.

The regression line was ok in the old version of Fig. 5. The new Fig. 5 (as well as Figs. 4 and 7) differs from the old one (as a result of the switch from *ambient* to *dry particle* number and surface area concentrations).

Reviewer #2

General comment

This paper discusses the potential for estimating the particle number concentrations of cloud condensation nuclei (CCN) and ice nuclei (IN) and the particle surface area concentration from the polarization lidar measurement. The estimation method of the conversion parameters from particle extinction coefficient to number and surface concentrations solely based on the ground-based Sun-sky radiometry (AERONET) measurements. It measures the sun and sky radiance at several wavelengths from which spectral aerosol optical thickness and particle volume distributions are retrieved. I think that the method is reasonable and logically consistent. However, I strongly suggest that it should be validated by comparing with the in-situ measurements of CCN and IN concentrations (as the authors mentioned in the Conclusions) because there might have large uncertainty in the particle number concentration retrieved from the Sun-sky photometry measurements. In particular, the number concentration with radius smaller than 0.1e-6 m, which contributes largely to N_CCN, has large uncertainty (Please see Figs. 1 and 8 and Table 4 in Dubovik et al., JGR, 2000). Thus, the authors should be careful about the estimate of the uncertainty in the NCCN retrieved using the method proposed in this paper.

The reviewer is right. As a consequence and as a first action, we checked the AERONET data again for artifacts in the determination of n_{50}, n_{60}, and n_{100} , and we found significant errors in the AERONET data base for Morocco (SAMUM-1, close to the desert dust source regions, bad numbers for the radius classes from 50-100nm). We no longer consider the Morocco data in the calculations of the desert dust conversion parameters (see for example Fig.6 in Sect. 4.2, the top panels now only show trustworthy data for Cabo Verde and Barbados, we checked all the field campaign data carefully again and again, and came to the conclusion to leave out the Morocco data completely in the computation of the conversion parameters in Table 3).

Just to mention that, in the revised version we now switch from ambient to dry-particle number concentrations (as input for the CCN and INP retrievals) so that for 60% (typical continental PBL relative humidity) and 80% RH (typical RH in marine PBL), the number concentration of n_{60} (radius > 57 nm, continental aerosol) and n_{100} (radius > 100nm, marine aerosol) are the proxies for dry-particle number concentrations $n_{50,dry}$. And in the case of desert dust the CCN input value is now n_{100} instead of n_{50}. This change towards larger particle sizes relaxes the situation concerning the errors in the CCN retrieval a bit.

Nevertheless, the next paper is already in progress where we will compare out lidar-based n_{CCN} profiles with measurements (as stated in the conclusions, now in more detail). We already did first comparisons, which are promising.

Furthermore, we already tried to include comparisons of our CCN-related correlation products with published ones (Shinozuka et al., 2015, Sakai et al., 2013, see Sect. 4.1, 4.2, 4.3). We include Shinozuka profiles in the lidar profile figures shown in the case study section 5.1. Shinozuka et al. (2015) allows us to compare data sets separately for marine, desert, and continental aerosol particles. A reasonable agreement is always given. Discrepancies can be explained by the fact that the Leipzig and Limassol data clearly indicate that these observations were done at urban sites (strong fine mode impact), whereas the Shinozuka and Sakai observations were done at sites with more background-like aerosol conditions (less fine-mode dominated). But to be very clear, we will do extensive comparisons with airborne in situ observations in future, based on already available data. We will also design future campaigns (in 2017) in that way that CCNC and INPC are measured with

aircraft around our lidar laser beams.

Regarding the error discussion, as suggested by the reviewer, we include the Dubovik et al. (2000) paper and provide a much better and satisfying error discussion in Sect. 2.1.

There is one more thing that I am wondering is that it does not discuss the detection limit of N_INP that is usually an order of 1 Lˆ−1 in the real atmosphere and the contribution of the backscattering to the total backscattering coefficient is very small. Thus, I suggest the authors to add discuss these topics in the paper.

We did not include such a discussion. We estimate n_{INP} and n_{250} from the lidar-derived extinction coefficient. If there would be a detection limit in the lidar measurement then we would also have a detection limit in the n_{INP} retrieval. But we do not have such a detection limit for extinction coefficients. If the retrieved extinction values get more and more noisy with decreasing extinction strength, then we increase vertical smoothing and temporal averaging. We can still identify rather thin and fine traces of aerosols up to great heights…. It simply depends on smoothing and averaging. This is the reason why we do not provide a discussion on detection limits.

Specific comments

1) ***P34160, L15: Please explain how you estimate the magnitude of contribution of marine particles to the measured non-dust backscatter coefficient.***

We explain that now in much more detail (Sect. 3.1 and 3.4.1), how we handled the marine contribution to backscatter and extinction coefficients. But we do not have a clear idea and answer! So, we keep the discussion simple. The main message is: We assume a marine contribution to extinction in the marine PBL (over oceanic, 100%, and over small islands as Cyprus and at coastal sites), but not in the PBL over continental sites (as over Leipzig). We neglect a marine contribution to extinction in the free troposphere in general (over the oceans and over the continents). We discuss this point based on our numerous profile observations over remote oceanic sites, and we provide numbers of the extinction contribution in the free troposphere in Sect. 3.4.1. The contribution of free-tropospheric marine particles to the CCN and INP budget is usually rather small according to our lidar observations.

2) ***P34172, L27: Did you check the particle imaginary refractive index retrieved from AERONET measurements to examine the different absorption contribution to the particle extinction coefficient? Please comment on it if possible.***

No we did not make such an attempt.

3) ***P34176, L26: To compute the continental pollution extinction coefficient, did you use a constant lidar ratio over height or vary with height between 50 and 60 sr?***

We always assumed a height-independent lidar ratio in the studies presented here.

4) ***P34176, L26: Please give the lidar ratio for marine particle in Fig. 8. In addition, please provide the lidar ratio values used for 355 nm.***

This is given for 532nm in Fig. 2, on which Figs. 8 and 9 are based. Note, that the 355 nm case is now removed from Fig. 8 in the revised version.

5) ***P34177, L26: It might be helpful to refer the paper by Sakai et al. (2014) that compared the lidar observations with respective airborne in-situ observation of CCN and aerosol particles.***

Yes, we included this interesting paper (Sakai et al., JMSJ, 2013). We find partly good agreement (n_{150} vs n_{250} , Sect. 4.1), but also realized that the CCN-backscatter correlation shows more background-like conditions (Sect. 5.1) over the field site in southern Japan, when compared to our urban Limassol and Leipzig data. To be sure that the Leipzig CCN conversion data are ok, we checked several

measurements of horizontal long-path extinction observations (close to our institute, 3km long path, Skupin et al, ACP, 2016) performed together with particle size distribution observations, and found that n_{50} is 1000-2000 cm^{-3} for ambient extinction coefficients of 75-150 Mm^{-1}. So, this agreement supports the usefulness of our CCN retrieval approach.

6) Table 3: Please provide the standard deviation for C_p50, if possible. Technical correction

Now given in Table 3.

7) Fig. 9: I cannot distinguish thick and thin lines in the left panel.

This figure is changed. We no longer show profiles for different supersaturation levels (no longer thick and thin lines here).

References

Dubovik, O., A. Smirnov, B. N. Holben, M. D. King, Y. J. Kaufman, T. F. Eck, and I. Slutsker (2000), Accuracy assessments of aerosol optical properties retrieved from Aerosol Robotic Network (AERONET) Sun and sky radiance measurements, J. Geo- phys. Res., 105(D8), 9791–9806, doi:10.1029/2000JD900040.

Sakai, T., T. Nagai, N. Orikasa, Y. Zaizen, K. Yamashita, Y. Mano, and M. Mu- rakami (2014), Aerosol Characterization by Dual-Wavelength Polarization Lidar Mea- surements over Kochi, Japan during the Warm Seasons of 2008 to 2010, J. Meteoro- logical. Soc. Jpn., 91, 789–800, doi:10.2151/jmsj.2013-605.

These references are now included.

Reviewer #3:

General Comment

… I list a number of minor comments, and a couple major ones.

The first major point is that the authors have used a parameterization to represent pollution INPs that was developed based on data that appears not at all to have included strong anthropogenic pollution influences. In fact, it appears to have effectively isolated such influence by restricting relation only to aerosols larger than 500 nm diameter in regions away from urban areas where those number concentrations never exceeded about 10 per cc, and then appear likely the consequence of sampling mineral dust aerosols. This application of the DeMott et al. (2010) parameterization for pollution for the first time is a misstep, one that could then be erroneously referenced as indicating that pollution particles are efficient INPs, perhaps as efficient as mineral dust under some conditions. This has never been shown using actual data to my knowledge, and if such data did exist, then surely evidence would be widespread throughout the ice nucleation literature. It is not. I suggest that, alternately, this parameterization could be used as a contrast to others that are purely for mineral dusts, but should not be ascribed in any manner to pollution particles. I do not know if that is possible, or if it meshes with the lidar profiling that has been done. I will guess that this is problematic for the authors because they are using the lidar response to anthropogenic haze and biomass smoke specifically for a category termed "continental pollution" aerosols. The solution to this problem is not clear, unless specific parameterizations are proposed for smoke and/or pollution on the basis of data in the literature.

We agree! It was misleading to use 'aerosol pollution' instead of a more precise description such as 'non-desert continental aerosol'. Pollution means more or less: fine mode aerosol. We understood the general message of the reviewer... Therefore: In the revised versions we only have the following three aerosol types: marine particles, desert dust, the non-desert continental aerosol which includes urban

haze, biomass burning smoke, but also ***soil and road dust***, and biogenic particles. This is mentioned in Sect.1 for the first time and then repeated several times throughout the paper. We purged all 'aerosol pollution' statements.

This non-desert continental aerosol (which comprises all terrestrial particles except the desert dust component) contains mineral dust traces.These traces of dust may be widely responsible for the INP efficacy of this aerosol type, besides biological particles and some 'strange components' of the industrial aerosol cocktail over polluted continents.

So, in the next step (Sect. 3.4.1), we argue that the DeMott et al. (2010) INP parameterization is applicable to our aerosol type 'non-desert continental aerosol'. We mention that the DeMott 2010 paper is based on many continental field campaigns (4 in Colorado, 2 in Eastern Canada, 1 in Amazonia, 1 in Alaska) and we argue that such a parameterization then should be applicable to European continental aerosols as well, and not only to North American or even Asian continental aerosol mixtures. We clearly believe that the DeMott et al. (2010) INP parameterization is the best we have in the literature to describe the overall INP behavior of non-desert continental aerosol mixtures.

And when we check our own lidar observations of ice containing clouds over Europe (Seifert et al., JGR, 2010) we always find that the two parameterizations (DeMott 2015 for desert dust and DeMott 2010 for non-desert continental aerosols) well explain many features we observe with lidar over Europe (Sect. 3.4.1). Many ice containing clouds already occur in the temperature range from -5 to -15°C). Desert dust is, however, almost not active at these high temperatures, in agreement with the DeMott (2015) parameterization.

A few other key things needing attention in my opinion are:

1) ***It would be useful to introduce the fact that aerosol numbers are not corrected for RH growth that may be present in the ambient observations. That is, dry aerosol distributions are not used.***

This was a rather useful and valuable comment! This statement triggered the most significant change of the entire paper. Now, we consider the water uptake effect in the methodology.

We explain how we consider this effect in detail in Sect. 3.2. Briefly summarized, we ignore a potential water uptake effect in the case of hydrophobic desert dust (so nothing changed here). We assume an RH of 60% (typical continental PBL relative humidity) and 80% RH (typical RH in marine PBL), so that the number concentration of n_{60} (radius > 57 nm, continental aerosol) and n_{100} (radius > 100nm, marine aerosol) are now the proxies for dry-particle number concentrations $n_{50,dry}$. Furthermore , in the case of hydrophobic desert dust the CCN input value is now n_{100} instead of n_{50} (see Sect . 1 and 3.3 for explanations). In the INP parameterization, we have n_{250} (for dust), n_{290} (for continental), and n_{500} (for marine particles) as proxies for $n_{250,dry}$. Which is the particle number concentration for dry particles with dry particle radius > 250nm.

The choice of n_{60}, n_{100} , n_{290} , and n_{500} is motivated by the assumption that particles grow by a factor of about 1.15 (when RH increases from 0% to 60% for continental particles at typical mean RH conditions in the continental PBL) and by about 2 (when RH increase from 0% to 80% in the case of sea salt at typical RH conditions in the marine PBL). New conversion factors are determined by correlating n_{60}, n_{100} , n_{290} , and n_{500} with the lidar-derived extinction coefficient (for ambient conditions) in Sect. 4 (and here Figs. 4-5). All these new conversion factors are considered in the equations in Sect. 3.

We are aware of the fact, that our parameterizations now only hold for certain RH conditions (+/- 20%) …. and we discuss this aspect in Section 5. We now show temperature and RH profiles in Figs. 9 and 11 in Sect. 5 to better discuss the RH influence.

It is clear also that our paper is open for discussion because of the many assumptions we have to make, and that we need comparisons with airborne CCN and INP observations to get a good characterization of the potential and limits of the applied lidar methods and of the quality of the obtained results.

2) Terminology for relevant quantities should be unified throughout the paper (see specific comments)

We agree, and did this time consuming work. All in all, it was a good idea to force us in this direction.

3) The parameterization of Steinke et al. (2015) is applied for deposition nucleation, but with little concern for the fact that that study exclusively focused on Arizona Test Dust as the basis for the parameterization. It is widely known in the ice nucleation community that ATD is not a good atmospheric dust surrogate. Consequences seem apparent in the results given here, yet no qualifications are given.

This is now mentioned in Sect. 3.4.2, and also in Sect. 5.1 (dust outbreak case study).

Specific comments

1. Introduction

Page 34152, line 1: After introducing the shorthand APC for aerosols and CCN, why not use it for INP, for example AP CI N P instead of creating an alternate form (INPC)? Furthermore, a more standard notation (nI N P) is used in section 3. Are there reasons not to use a single notation, preferably the latter form, from the beginning of the paper?

Triggered by these statements we changed the notation completely and only have: n_{50}, n_{60}, n_{100}, n_{250}, n_{290}, n_{500}, n_{CCN}, $n_{INP.}$

Page 34152, line 5: The same issue is present for CCNC versus (AP CC C N already defined, and nCCN,xx

We now use always: $n_{CCN,ss,i}$ (with ss for supersaturation, and i for aerosol type)

Page 34152, lines 11-12: Please explain what is meant by mineral dust particles being fully activated below -20 ◦C. Many studies, including Murray et al. (2012) indicate that nucleation is not fully stochastic for all INP and that the active fraction and site density for many mineral dusts are strongly temperature dependent even below -20 ◦C. Hence, I believe this statement to be false.

We changed that! Instead of … fully activated…. , we now state: …. are favorable INP ….

Page 34152, lines14-17: Herein starts a problem in including a variety of aerosol types, indistinguishably with regard to ice nucleation, as "continental particle mixtures" that always contain efficient INPs. While it is certainly true that all of these particle types are emitted from continents, they are distinct types that need distinct definition as INPs. This problem becomes a flaw when it is later assumed that the DeMott et al. (2010) parameterization can encapsulate these specific sets of sources, and pollution ("an thropogenic haze") INPs in particular. I will elaborate on this below.

We agree, and extend a bit the discussion on the impact of uncertainties caused by the unknown aerosol chemical compositions (or unknown contribution of different aerosol types). This is done in Sect. 3.4.1, after introducing Eq.13. The reason for the large uncertainties (factor of 5-10) is related to the unknown aerosol INP-relevant chemical and morphological properties. We provide more references which are pointing to the weakness of the DeMott (2010) parameterization (McCluskey et al., 2014, Mason et al., 2015, 2016, Taylor et al., 2016a, 2016b, and Murray et al., 2012). But we still think that this DeMott (2010) parameterization, derived from 9 continental measurement campaigns, is

an appropriate INP parameterization scheme for continental aerosol mixtures (as long as we do not have better parameterizations…). In the reality of lidar monitoring, it is practically impossible to obtain reliable information on the actual aerosol type mixture…., so we have to live with large uncertainties in the INP profiling. And this is not restricted to remote sensing.

Page 34153, line 16: Where do soil dust particles fit (soil and road dust mentioned on the last page)? Are these assumed the same as mineral dusts? Reducing this category now to anthropogenic haze and smoke mixtures is unfortunate, as smoke particles have been identified (though not parameterized) as INPs in published studies (e.g., McCluskey et al., 2014), while little or no data exists for anthropogenic particles contributing as INPs at mixed phase cloud temperatures in the free troposphere (unless the authors can prove so). There is stronger evidence for sources of organic and biogenic INPs from soils and plants that are present in air over continents at sizes above 500 nm.

As mentioned, to be clear throughout the paper: we avoid to say: 'aerosol pollution' or 'anthropogenic particles'. We always state: 'non-desert continental aerosol' and often give the full defintion… that this aerosol contains haze, smoke, soil and road dust, biological particles.

We separate the 'desert dust' aerosol type (showing high depolarization ratios of 30%) from the 'continental aerosol' type (showing low depolarization ratios <5%). The polarization lidar is only able to distinguish desert dust layers form the rest. The weak depolarization in the case of continental aerosol is caused by traces of nonspherical soil and road dust. Even some large biological particles may cause weak depolarization because of their non-spherical shape.

The comparably high smoke INP efficacy (McCluskey 2014) is probably caused by soil dust injected in to the atmosphere by the hot burning fires and related high turbulence close to the surface.… All in all, we all have the same difficulties: We do not know the exact aerosol composition if we go into the field and then we have to live with large uncertainties because of the unknown aerosol-type composition.

Page 34154, line 9: Can you explain what is meant by a simulation study? Does that mean using a global aerosol model as ground truth? If so, please state so.

We explain that now in more detail in Sect. 1. In the simulation study, one models the optical properties of a large number of different particle concentrations, chemical compositions, and different particle size distributions. Afterwards the simulated particle number concentration (calculated from the assumed particle size distributions) can be correlated with the computed particle extinction coefficients to see how feasible that is to obtain the microphysical properties from the extinction coefficients.

2. Instrumentation

Page 34158, lines 10-13: These statements bring to mind for the first time that these numbers could drastically differ depending on RH, and to this point in the paper, nothing is said about how this factor is dealt with.

So, now the water uptake effect is fully included in the methodlogy. And the comparisons in Sect. 4.1-4.3 with in situ measurements of CCNC and particle extinction coefficients (and their correlation) published by Shinozuka et al. (2013) corroborates that our approach (including the water uptake corrections) is ok.

3. Methodology

Page 34162: Is some typical hygroscopicity value assumed in (4) to (6)? And doesn't one require dry sizes first, prior to computation of CCN number?

This comment convinced and pushed us to go for dry-particle number concentrations (Sect.3 and 4). The CCN and INP parameterizations are now based on dry-particle information in the revised version.

Page 34163: Absent a mention of assumed composition, it is not clear where the supersaturation associated with APC40 comes from.

In Sect. 3, in the first paragraph, we now give a more general introduction what parameters and conditions determine n_{CCN}. And here we state that updraft strength determines the supersaturation level. We provide several publications which support this. These publications indirectly indicate that the chemical composition obviously plays a second-order role regarding the critical activation radius.

Page 34164, line 8: There is no justification given (and none possible in my opinion) for using the parameterization of DeMott et al. (2010) for continental pollution for the reasons already stated. Projects are listed in the DeMott et al. supplemental section that include mineral dust influences, but none for which pollution was a key type, and the creation of an INP surrogate via particles larger than 500 nm appears to have been done specifically to avoid pollution if possible (considering the impacts of pollution on such INP-size relationships evident in Richardson et al, 2007, referenced by DeMott et al., 2010). Figure S1 in DeMott et al. (2010) shows a range of aerosol concentrations that does not seem to reflect what might occur for heavily polluted air. It is likely that data and sampling scenarios from that figure are available, and could be used to assess if any pollution influences were included in that "global" parameterization. That it may not be the case always that pollution particles stay at diameters below 500 nm creates a dilemma for generally applying the D10 parameterization, but one that has to be stated as a dilemma nonetheless, not solved by assuming that the parameterization is valid for pollution. The parameterization can be used as a contrast for a more globally-averaged INP, but cases where it is falsely enhanced by pollution should be specially noted and probably omitted from consideration (problematic for this paper that creates a category for pollution, but with no data on INP to ascribe toward it).

Yes, as already mentioned above, the reviewer is right. We should avoid the impression that there is an aerosol type: ***aerosol pollution*** . This is misleading, the reader may believe we just a have fine-mode containing urban haze and fine-mode smoke, and that these fine-mode particles are good INP and can be described by the DeMott (2010) parameterization. We agree, this is simply not true. DeMott (2010) cannot be applied to POLLUTION.

To repeat again: As a consequence, we now clearly denote this aerosol type (throughout the paper): ***(non-desert) continental aerosol***, and several times we add in (…) : …..continental aerosol (haze, smoke, soil and road dust, biological particles). So we want to clearly state that we just distinguish desert dust from the residual terrestrial aerosol. And we know (or better believe) that INP is always directly linked to large particles. So, aerosol pollution (only fine-mode) is not a good definition when talking about INP.

As was stated already: We also explicitly list all the field campaigns (Sect. 3.4.1), on which of the DeMott et al. (2010) parameterization is based on. And if we then have the definition for our aerosol type (which includes the coarse mode fraction) then we feel: It is justified to take the DeMott(2010) INP parameterization for this kind of aerosol, in North America (most field campaigns were in Colorado and eastern Canada) as well as in Europe.

Page 34165, line 1: Wex et al. (2014) do not discuss ice activation by purely anthropogenic particles, just coated ones. Please correct. In fact, this surrogate coating for anthropogenic organic particles has no active impact (positive) on ice activation in the temperature regime examined.

We add: ….According to Wex et al. (2014) ice nucleation for anthropogenic particles ***(with an insoluble part)*** and coated mineral dust particles anthropogenic particles……. The rest is ok, we believe.

Page 34165: It is necessary to note that the parameterization of Steinke et al. is for Arizona Test Dust, an atmospheric surrogate that exceeds the INP activation proper- ties of Asian or

Saharan dust (see, e.g., Niemand et al. 2012). This probably explains the overactive deposition process in figures shown in this paper in comparison to im- mersion freezing by mineral dust.

We mention this now when we present the equation (in Sect. 3.4.2) and later when we use the parameterization (Sect. 5.1, case study)

Page 34166, lines 1-4: Justification for the statements made here is not given, and these statements are problematic. Why assume a constant SS_ICE , when this is a variable? How is Steinke et al. (2015) applied for pollution? These particle types were not examined by those authors. The lack of detail and discussion here is unacceptable.

Without a knowledge of the actual ss_ICE value we have to set ss_ICE to a typical value. We selected a typical (but moderate) value of 1.15 according to Comstock et al. (2008). We changed the text accordingly in Sect. 3.4.2. We skipped the sentence regarding pollution. Only the dust INP retrieval option is mentioned.

4. AERONET observations of the relationships of APC and ASC with AEC

Page 34168: Were RH effects removed somehow? The title of Shinozuka et al. (2015) implies use of dry particle size, but that is not the case here. I could not resolve your discussion of any implications for the present study.

The CCNC observations of Shinozuka et al. (2015) were done at supersaturation values of 0.3-0.5% and the extinction coefficients were measured for dry particles. So we multiplied the extinction values by 1.4 (60% RH) and the CCNC values were divided by a factor of 2, to come close CCNC values for 0.15-0.2% supersaturation. After these manipulations, we computed CCNC values for given ambient extinction coefficients (Shinozuka 2015 observations) and compared these values with our results. This is explained in Sect. 4.1.

5. Lidar estimates. . .

Page 34175: Please explain better the reason for shifting the temperature profile by 15K. Is it meant to mimic the presence of similar aerosols at lower temperature? D10 is not for pollution though, so omit or apply only the dust number to it. That would be justified.

We skipped this part and also the Figure (Fig. 10 in the submitted version).

Again, we do not know a better parameterization (as D10) that we could use for non-desert continental aerosol (mixtures of anthropogenic haze, biomass burning smoke, soil and road dust, and biogenic particles) …. As explained above, after a more clear defintion of the non-desert continental aerosol type we think the use of D10 parameterization is justified.

Page 34175 and Figures 9 and 10: The higher values in N12 versus D15 could result from substantial ASC existing below a radius of 250 nm, as stated, but could also relate to the failure to convert to dry size distributions before comparing a parameterization based on size with one based on surface area.

Even after switching from the old method with aerosol parameters for ambient conditions to the new one for dry particle number concentrations and surface area concentrations, the discrepancy between D10 and N12 remains. Our recent attempts (closure between ice crystal number concentration (ICNC) of cirrus layers embedded in dust, and dust INPC around the cirrus) shows that D10 better matches the ICNC numbers.

Page 34175 and Figure 10: Why is the S15 parameterization shown for temperatures warmer than it is specifically valid. This is an issue because deposition does not typically occur for these conditions, at least on the basis of laboratory observations (i.e., it is a more typical behavior in the cirrus temperature regime). Then one wonders why S15 exceeds N12. This is

partly a difference in INP type and partly because it is probably invalid to plot S15 at these conditions.

We now show the S15 curve for the valid temperature range, only (Fig.9).

6. Conclusions

This section now requires revision for the discussion about pollution. Although the lidar may detect it, one cannot escape the fact that INP parameterizations have not been developed specifically for pollution. More likely, they have been developed to avoid it, because it does not represent a very efficient INP source and so is extremely poorly characterized. Similarly, the lidar may detect biomass burning layers, but the authors should then perhaps work with others who have collected data for such particles in order to apply a specific parameterization. These are clear current weaknesses in this paper, and clear future needs that should be discussed.

After all the changes, the conclusions are completely rewritten. And we mention that there is room for improvements. We give a long list of points that must be solved and improved. One point is the development of better aerosol-type dependent INP parameterizations.

McCluskey focused on INPs for biomass burning smoke. But also in that paper at the end they asked: May be soil particles (injected into the troposphere by the hot fires) were responsible for the unexpectedly enhanced INP numbers. So it remains difficult with the INP parameterization… in the field.

Technical editorial comments

Page 34151, line 13: "can be used" for "is requested"

Done!

Page 34152, line 10: "efficacy"

Is now corrected, several times…

Page 34156, lines 15-16: please note that this sentence repeats the first sentence of this section.

The complete section 2.1 is changed, and this repeating statement is now removed…

Page 34158, lines 6-9: Suggest rewriting for awkward language as, "ASC from AERONET is almost 98

Changed!

Page 34159, lines 6-7: "profiles" repeats. Remove one.

Done!

Page 34161, line 26-27: remove "to introduce"

The full sentence is skipped.

Page 34162: Begin sentence "Determination of the specific. . ."

Done!

Page 34162: Again, use of multiple terms to define the same quantities inside and outside of equations here is very confusing and unnecessary. Section 3.3 even amends the APC term to

include supersaturation now, but this could have been done at the beginning of the paper. Nevertheless, it is again redefined starting in Eq. 4.

All this now solved (we hope) as suggested by the reviewer…. We significantly simplified the entire notation. But we avoid to introduce all the indices already in the introduction…. We introduce them step by step when they are needed…

Page 34163, line 10: missing "our" before "own".

Done!

Page 34165, line 11: replace "leave out to" with "do not".

No longer needed. We included a discussion on marine particles in the revised version….

Page 34172, line 12: use "disturb" for "disturbed"

Also not needed to improve…, the revised version does no longer contain this sentence…

Page 34175, line 7: replace "after" with "of"

Done!

References

McCluskey, C. S., P. J. DeMott , A. J. Prenni, E. J. T. Levin, G. R. McMeeking, A. P. Sullivan, T. C. J. Hill, S. Nakao, C. M. Carrico, and S. M. Kreidenweis, 2014: Characteristics of atmospheric ice nucleating particles associated with biomass burn- ing in the US: prescribed burns and wildfires, J. Geophys. Res. Atmos., 119, doi:10.1002/2014JD021980.

Is included in the revised version

Richardson, M. S., P. J. DeMott, S. M. Kreidenweis, D. J. Cziczo, E. Dunlea, J. L. Jimenez, D. S. Thompson, L. L. Ashbaugh, R. D. Borys, D. S. Westphal, G. S. Cassucio and T. L. Lersch, 2007: Measurements of heterogeneous ice nuclei in the Western U.S. in springtime and their relation to aerosol characteristics. J. Geophys. Res., 112, D02209, doi:10.1029/2006JD007500.

Is not included in the revised version, however, often cited in previous papers published by TROPOS authors.

Manuscript prepared for J. Name
with version 4.2 of the LaTeX class copernicus.cls.
Date: 27 March 2016

Potential of polarization lidar to provide profiles of CCN- and INP-relevant aerosol parameters

R. E. Mamouri[1] **and A. Ansmann**[2]

[1]Cyprus University of Technology, Dep. of Civil Engineering and Geomatics, Limassol, Cyprus
[2]Leibniz Institute for Tropospheric Research, Leipzig, Germany

Abstract.

We investigate the potential of polarization lidar to provide vertical profiles of aerosol parameters from which cloud condensation nucleus (CCN) and ice nucleating particle (INP) number concentrations can be estimated. We show that height profiles of particle number concentrations $n_{50,\mathrm{dry}}$ considering dry aerosol particles with radius $> 50\,\mathrm{nm}$ (reservoir of CCN in the case of marine and continental non-desert aerosols), $n_{100,\mathrm{dry}}$ (particles with dry radius >100 nm, reservoir of desert dust CCN), and of $n_{250,\mathrm{dry}}$ (particles with dry radius >250 nm, reservoir of favorable INP), as well as profiles of the particle surface area concentration s_{dry} (used in INP parameterizations) can be retrieved from lidar-derived aerosol extinction coefficients σ with relative uncertainties of a factor of 1.5-2 in the case of $n_{50,\mathrm{dry}}$ and $n_{100,\mathrm{dry}}$ and of about 25–50 % in the case of $n_{250,\mathrm{dry}}$ and s_{dry}. Of key importance is the potential of polarization lidar to distinguish and separate the optical properties of desert aerosols from non-desert aerosol such as continental and marine particles. We investigate the relationship between σ, measured at ambient atmospheric conditions, and $n_{50,\mathrm{dry}}$ for marine and continental aerosols, $n_{100,\mathrm{dry}}$ for desert dust particles, and $n_{250,\mathrm{dry}}$ and s_{dry} for three aerosol types (desert, non-desert continental, marine) and for the main lidar wavelengths of 355, 532, and 1064 nm. Our study is based on multiyear Aerosol Robotic Network (AERONET) photometer observations of aerosol optical thickness and column-integrated particle size distribution at Leipzig, Germany, and Limassol, Cyprus, which cover all realistic aerosol mixtures. We further include AERONET data from field campaigns in Morocco, Cabo Verde, and Barbados, which provide pure dust and pure marine aerosol scenarios. By means of a simple CCN parameterization (with $n_{50,\mathrm{dry}}$ or $n_{100,\mathrm{dry}}$ as input) and available INP parameterization schemes (with $n_{250,\mathrm{dry}}$ and s_{dry} as input) we finally compute profiles of the CCN-relevant particle number concentration n_{CCN} and the INP number concentration n_{INP}. We apply the method to a lidar observation of a heavy dust outbreak crossing Cyprus and a case dominated by continental aerosol pollution.

Correspondence to: R. E. Mamouri (rodanthi.mamouri@cut.ac.cy)

1 Introduction

Field studies of aerosol-cloud-dynamics interaction are presently in the focus of atmospheric research. Large uncertainties in weather and future-climate predictions (IPCC, 2013) arise from gaps in our knowledge of the detailed impact of aerosols on the evolution of liquid-water, mixed-phase and cirrus clouds. This unsatisfactory situation motivates the strong efforts presently undertaken to investigate formation and evolution of cloud layers and associated aerosol-cloud interactions.

Aerosol particles influence cloud evolution, lifetime, and cloud microphysical properties in two ways. Aerosol particles can serve as cloud condensation nuclei (CCN) in liquid droplet nucleation processes and/or as ice-nucleating particles (INP) in ice nucleation processes which include also the conversion of liquid droplets into ice crystals (immersion freezing). Ground-based active remote sensing (lidar and radar observations) can be used to continuously monitor the evolution of clouds in their natural environment, at given meteorological conditions with high vertical and temporal resolution (Illingworth et al., 2007; Shupe, 2007; Ansmann et al., 2009; de Boer et al., 2011; Schmidt et al., 2014).

Lidar is the most prominent tool for aerosol profiling in terms of particle optical properties. However, to improve the study of aerosol-cloud interaction, the potential of lidar to provide vertical profiles of particle number concentrations such as $n_{50,\mathrm{dry}}$ considering all dry particles with radius $> 50\,\mathrm{nm}$ (reservoir of favorable CCN in the case of marine and anthropogenic particles) (Quinn et al., 2008; Rose et al.,

2010; Deng et al., 2011), $n_{100,\mathrm{dry}}$ (dry particles with radius $> 100\,\mathrm{nm}$, reservoir of favorable CCN in the case of desert dust) (Koehler et al., 2009; Kumar et al., 2009, 2011), or of the large particle fraction $n_{250,\mathrm{dry}}$ (all particles with dry radius $> 250\,\mathrm{nm}$, reservoir of favorable INP) (DeMott et al., 2010, 2015), needs to be explored in detail. The central question of our study is: Can we use lidar-derived vertical profiles of aerosol backscatter coefficient β and extinction coefficient σ, measured at ambient relative humidity conditions, to estimate vertical profiles of dry particle number concentration n_{dry} and surface area concentration s_{dry} from which the cloud-relevant particle number concentrations n_{CCN} (indicating the CCN particle reservoir) and n_{INP} (INP number concentration) can be estimated?

A first promising feasibility study regarding the retrieval of n_{INP} profiles from lidar observations was undertaken by Mamouri and Ansmann (2015). Former studies indicate also that measured aerosol optical properties (at wavelengths around 500 nm) can be used to estimate CCN number concentrations, CCNC (Ghan and Collins, 2004; Ghan et al., 2006; Andreae, 2009; Jefferson, 2010; Liu and Li, 2014; Shinozuka et al., 2015).

A crucial point regarding n_{CCN} and n_{INP} profiling is that the efficacy of aerosol particles to act as CCN or INP depends on aerosol type. In the case of heterogeneous ice nucleation it is found that mineral dust particles are favorable INP at temperatures below about $-20\,^{\circ}\mathrm{C}$ (Ansmann et al., 2009; Murray et al., 2012; Augustin-Bauditz et al., 2014), that marine particles seem to be comparably inefficient INPs (Kanitz et al., 2011) at temperatures $> -25\,^{\circ}\mathrm{C}$, whereas continental aerosols (mixtures of anthropogenic haze, biomass burning smoke, soil and road dust, and organic and biogenic particles from soils and plants) seem to contain always a significant amount of efficient INPs, already leading to ice nucleation at temperatures as high as -5 to $-15\,^{\circ}\mathrm{C}$ (Seifert et al., 2010; Zhang et al., 2010; Kamphus et al., 2010; Ebert et al., 2011; Augustin et al., 2013; Hartmann et al., 2013; Bühl et al., 2013; Pummer et al., 2015; Umo et al., 2015).

In the case of cloud droplet formation, we have to distinguish at least desert dust and non-desert particles (continental and marine aerosol components) (Koehler et al., 2009; Kumar et al., 2009, 2011; Karydis et al., 2011; Bangert et al., 2012). Marine and hygroscopic continental particles with dry radius >50 nm get activated even at low supersaturation of 0.1-0.2% (i.e., at relative humidities over liquid water of 100.1 to 100.2%), whereas the critical activation radius of hydrophobic insoluble desert particles with a negligible amount of soluble material (coating) on the surface is >100 nm (Koehler et al., 2009; Kumar et al., 2011). Thus, lidar must be able to separate these basic aerosol types and to provide n_{CCN} and n_{INP} profiles separately for marine, non-desert continental, and desert dust aerosols.

In principle, multiwavelength Raman/polarization or high-spectral-resolution (HSR)/polarization lidars can provide the desired microphysical particle properties (Müller et al., 2005; Veselovskii et al., 2010; Müller et al., 2013, 2014). However comparably complex lidars and comprehensive data analysis methods as well as a good knowledge in the use of ill-posed inversion techniques are required to make these efforts successful. For this reason, we investigate an alternative approach. The overall goal is to develop a robust and easy-to-apply method that allows fast computation and implementation of an automated code in the lidar aerosol and cloud data analysis software. Thus, the method should be simple and applicable to single-wavelength lidar observations at 355, 532, or 1064 nm wavelength to estimate profiles of particle number concentrations $n_{50,\mathrm{dry}}$, $n_{100,\mathrm{dry}}$, $n_{250,\mathrm{dry}}$, and surface area concentration s_{dry} for the three basic aerosol types. Many lidars are single-wavelength lidars (e.g., 355 or 532 nm backscatter lidars) including the upcoming space lidars of the European Space Agency operating at 355 nm (Ansmann et al., 2007; Illingworth et al., 2015a) which are planned to be launched within the next 1–3 years. Furthermore, a dense European single-wavelength ceilometer network is developing, organized by European weather services (http://www.dwd.de/ceilomap) (Wiegner and Geiß, 2012; Wiegner et al., 2014; Illingworth et al., 2015b).

To make full use of the retrieval schemes presented in this article, polarization lidars (Freudenthaler et al., 2009) are of advantage. This is a key point of the entire study. By means of the polarization lidar technique, the desert dust aerosol component can be easily separated from other continental aerosol components as well as from marine aerosol. Desert dust causes high depolarization of backscattered linearly polarized laser light, whereas typical non-desert aerosol mixtures lead to very low depolarization. After the separation of the basic aerosol types, in the next step the particle number and surface area concentrations, required as input in the CCN and INP parameterization schemes, are separately determined from the lidar-derived particle extinction coefficients for the basic aerosol types (desert, marine, continental), as outlined in Sects. 3 and 4,.

The study presented here is based on our long experience in detection, separation, and quantification of optical and microphysical properties of different aerosol types by using polarization lidars in combination with sun photometers (Tesche et al., 2009, 2011; Ansmann et al., 2011b, 2012; Mamouri et al., 2013; Mamouri and Ansmann, 2014; Nisantzi et al., 2014, 2015). This study can be regarded as a follow-up effort of Mamouri and Ansmann (2015). However, in a much broader and more general sense, we now illuminate the potential of lidar to provide cloud-formation-relevant aerosol parameters for both liquid-water droplet and ice crystal nucleation. New aspects deal with the estimation of $n_{50,\mathrm{dry}}$ and $n_{100,\mathrm{dry}}$, the CCN parameterization, the retrieval of the particle surface area concentration s_{dry} from measured particle extinction coefficients, and the consideration of further dust INP parameterizations developed by Niemand et al. (2012) and Steinke et al. (2015), in

which the dust values of s_{dry} are input instead of $n_{250,\mathrm{dry}}$ (DeMott et al., 2010, 2015). In addition, new findings regarding the efficacy of marine particles to serve as INP are taken into account (DeMott et al., 2016). In the present study, the wavelength range is extended from 532 nm to all three relevant laser wavelengths so that the CCN and INP-relevant aerosol conversion parameters are available for 355 and 1064 nm as well.

The study makes use of multiyear photometer observations of the Aerosol Robotic Network (AERONET) (Holben et al., 1998) at Leipzig, Germany, Limassol, Cyprus, and at Ragged Point, Barbados. We further include AERONET data from desert dust field campaigns in Morocco, Cabo Verde, and Barbados. The main goal is to investigate the link between the microphysical particle properties such as $n_{50,\mathrm{dry}}$, $n_{100,\mathrm{dry}}$, $n_{250,\mathrm{dry}}$, and s_{dry} and the ambient particle extinction coefficient, measurable with lidar, for "real-world" aerosol conditions. Long-term AERONET observations reflect best the full range of occurring aerosol mixture and layering scenarios. An alternative approach would be an extended simulation study of the correlation between the cloud-relevant microphysical and measurable optical properties of the aerosol, similar to the study presented by Barnaba and Gobbi (2001) for marine and dust aerosols.

The paper is organized as follows: The AERONET stations and measurement products as well as the lidar sites and lidar products are given in Sect. 2. Section 3 presents our methodology to obtain profiles of $n_{50,\mathrm{dry}}$, $n_{100,\mathrm{dry}}$, $n_{250,\mathrm{dry}}$, s_{dry}, n_{CCN}, and n_{INP} from lidar profiles of ambient particle extinction coefficients σ for the three basic aerosol types (desert, marine, continental). The conversion of measured optical properties into particle number and surface area concentrations requires good knowledge of the correlation between optical and microphysical particle properties. This knowledge is gained from the mentioned long-term AERONET measurements and the specific dust field campaigns. The main findings of the AERONET-based correlation studies are presented and discussed in Sect. 4. Section 5 finally deals with the application of the developed methods to two lidar observations conducted during a strong desert dust outbreak towards Cyprus and during conditions with (non-desert) continental aerosol pollution over Cyprus. A summary and concluding remarks are given in Sect. 6

2 Instrumentation

In Sect. 2.1, we provide an overview of the AERONET stations, the basic AERONET products, and the retrieval of the column-integrated particle number and surface area concentrations. In Sect. 2.2, we briefly describe our lidar instruments.

2.1 AERONET sun/sky photometers

The study is based on the analysis of three long-term and four field-campaign AERONET data sets. We investigated 14 years of AERONET observations at Leipzig, Germany, performed by the Leibniz Institute for Tropospheric Research (TROPOS) from 2001-2015. Leipzig is a highly polluted central European city which is affected by Saharan dust outbreaks about 2-10 times per year (Mattis et al., 2004, 2008). We analyzed four years of AERONET observations at Limassol, Cyprus, performed by the Cyprus University of Technology (CUT) from 2011 to 2015 (Nisantzi et al., 2014, 2015). This site in the eastern Mediterranean is a unique station for aerosol studies. Aerosol mixtures of anthropogenic haze, biomass burning smoke, soil and road dust, and marine particles, and strong dust outbreaks from Middle East deserts and the Sahara frequently occur (Nisantzi et al., 2015). Our studies are complimented by AERONET observations conducted during the Saharan Mineral Dust Experiments SAMUM-1 (Ouarzazate, Morocco) (Toledano et al., 2009) and SAMUM-2 (Praia, Cabo Verde) (Toledano et al., 2011; Ansmann et al., 2011a), the Saharan Aerosol Long-range Transport and Aerosol-Cloud interaction Experiments SALTRACE-1 (at the Caribbean Institute for Meteorology and Hydrology (CIMH), Barbados, summer 2013) (Groß et al., 2015) and during SALTRACE-3 (Barbados, summer 2014) (Haarig et al., 2015). The field campaigns offer the unique opportunity to study the correlation between the particle optical properties (extinction coefficient σ, aerosol optical depth AOT) and the microphysical properties (column or layer mean values of, e.g., n_{100}, n_{250}, s) at pure dust conditions. During SALTRACE in 2013, even aircraft observations of CCNC in lofted dust layers in the Barbados area are available and the link between the in-situ-measured CCNC and the lidar-derived particle extinction coefficients will be discussed in a follow-up paper. Furthermore, we used 7.5 years of data from the AERONET station at Ragged Point, Barbados (level 2.0, 2007-2015) (Prospero and Mayol-Bracero, 2013) to study the correlation between the optical and microphysical aerosol properties for pure marine conditions. An overview of the observational periods and amount of available data for the analyzed different aerosol conditions with focus on the three defined aerosol types are given in Table 1. More details of these AERONET stations can be found on the AERONET web page (http://aeronet.gsfc.nasa.gov).

AERONET provides quality-assured products in terms of AOTs at up to 8 wavelengths (340 to 1640 nm) and column-integrated values for the Ångström exponent (AE, spectral dependence of AOT). From the AOT measurements and sky radiance observations at 4 wavelengths the column-integrated particle size distribution is retrieved (Dubovik and King, 2000; Dubovik et al., 2006), which then allows to compute particle volume concentration, surface area (column s), and column-integrated particle number con-

centrations n. All observations are performed at ambient temperature and relative humidity conditions. In Sect. 3.2, we will explain how we corrected for the particle water-uptake effect to obtain the required dry particle values, i.e., of $n_{50,\mathrm{dry}}$, $n_{100,\mathrm{dry}}$, $n_{250,\mathrm{dry}}$, and s_{dry}.

As explained in the methodology section 3, in the retrieval of n_{CCN} and n_{INP} we need to know the relationship between the observed (ambient) microphysical particle properties n_{50}, n_{60}, n_{100}, n_{250}, n_{290}, n_{500}, and s and the ambient particle extinction coefficient σ for desert dust, marine, and non-desert continental aerosol conditions. These relationships are quantified by means of the AERONET correlation studies for the particle extinction coefficients at 355, 532, and 1064 nm (Sect. 4). Because AERONET photometers do not directly measure AOTs at the laser wavelengths, we use the measured AOT at 380 nm and the Ångström exponent AE (340-380 nm) to obtain the AOT at 355 nm by interpolation. Similarly, in the case of 532 nm we use the measured AOT at 500 and AE (440-870 nm) to derive the 532 nm AOT. The AOT at 1064 nm is obtained by extrapolation based on the measured AOT at 1020 nm and AE (870-1020 nm).

The way to obtain the column-integrated particle number concentrations, e.g., the column values of n_{50} or n_{250}, from the basic AERONET information (column-integrated particle volume size distribution) is described in detail by Mamouri and Ansmann (2015) (see Sect. 3.2 and Fig. 3 in that article). The particle volume size distribution is retrieved for 22 logarithmically equidistant discrete radius points r_j with index j from 1 to 22 (Dubovik and King, 2000; Dubovik et al., 2006). The particle radius spectrum from r_1 = 0.05 to r_{22} = 15 μm is covered. Each radius r_j represents a radius interval of logarithmically equal width. To obtain the particle number concentration for each individual radius interval, we divide the determined volume concentration of a given radius interval (or for the discrete radius point r_j) by the volume of a single particle with radius r_j and multiply this ratio with the spectral integral width of 0.2716. Unfortunately, we left out this multiplication with the dimensionless spectral width in the foregoing paper (Mamouri and Ansmann, 2015) so that the presented number concentrations in Mamouri and Ansmann (2015) are a factor of 1/0.2716 (= 3.68) too high and also the respective conversion factor in Fig. 4 of that paper.

As outlined in Sect. 4, we need the column values of n_{50}, n_{60}, n_{100}, n_{250}, n_{290}, n_{500}, and s. The column value of the particle number concentration n_{50} is the sum of the number concentrations of all radius classes from 1-22 and thus covers the full size range of optically active particles. Similarly, the column n_{60} value is obtained by adding all particle number concentrations of the radius classes from 2-22 (particles with radius $>$ 57 nm). The column value of n_{100} considers the radius classes 4-22 (particles with radius >98 nm).

The INP-relevant column value of n_{250} is calculated as follows: This number concentration is the sum of the number concentrations of the radius intervals 8-22 plus an additional contribution by radius interval 7 (centered at r_7 = 255 nm). This additional contribution is obtained by calculating the mean number concentration of the two intervals 7 and 8 (centered at r_8 = 335 nm), assuming that this mean value represents the number concentration for the radius interval from 255 to 335 nm (centered at about 290 nm), and then taking 50% of the computed mean value to consider only one half of this size interval. This latter value is interpreted as the number concentration of particles with radius from about 250 to about 290 nm. Furthermore, we make use in Sect. 4 of n_{290} (radius classes 8-22, particles with radius $>$ about 290 nm), and n_{500} (radius classes 10-22, all particles with radius $>$ about 500 nm).

The total particle surface area concentration s is obtained by (a) computing the surface area of a sphere with radius r_j for all 22 radius intervals, (b) multiplying the obtained surface areas for the particles with radius r_j with the number concentrations of radius interval j (obtained from the foregoing calculations of n), and (c) calculating the total surface area concentration by adding all contributions of the 22 size classes up. According to airborne in situ observations of the particle size distribution during the SAMUM campaigns (Weinzierl et al., 2009), the AERONET-derived values of s for desert environments explain about 95% of the total surface area concentration (which includes particles with radius <50 nm). By inspection of all ground-based in-situ-measured size distribution at the urban site of Leipzig, taken during the full year of 2008, we found that s (from AERONET) is about 0.85 ($\pm$0.1) of the total s.

Dubovik et al. (2000) carried out a detailed analysis of uncertainties in the AERONET products. Caused by statistical signal noise, the uncertainties in the AERONET n_{50}, n_{60}, and n_{100} values can be as high as 20%. For the column values of n_{250}, n_{290}, n_{500}, and s, the uncertainties are around 10%. Offset errors (caused, e.g., by bad photometer pointing stability, by the use of wrong surface reflectance in the data analysis, and wrong AOT retrievals) can lead to extreme errors of the order of >50% for the column n and s values in individual observations. On average, uncertainties of 25-35% are expected. However, in the case of our multiyear AERONET observations with many calibration sessions (photometer calibrations in France or USA) and field campaign measurements with calibration session before and after the campaigns, strong biases and extreme uncertainties in our AERONET data sets can be ruled out. We assume in the following, that mean uncertainties in the used long-term and field-campaign mean values of the column values of n_{50}, n_{60}, n_{100}, n_{250}, n_{290}, n_{500}, and s values are about 10-20%.

2.2 Aerosol lidars

The AERONET station of CUT at Limassol is equipped with a polarization/Raman lidar and belongs to the European Aerosol Research Lidar Network EARLINET (Pappalardo et al., 2014). The CUT lidar is described by

Mamouri et al. (2013) and Nisantzi et al. (2015). The case study in Sect. 5.2 is based on the lidar observations at Limassol.

In Sect. 5.1, we discuss a lidar measurement obtained with a mobile system of the Polly$^{\mathrm{XT}}$ (POrtabLe Lidar sYstem, XT: extended version) series (Engelmann et al., 2015; Baars et al., 2015). This new Polly$^{\mathrm{XT}}$ was built by TROPOS for the National Observatory Athens (NOA) in 2014. The multiwavelength Raman/polarization lidar was extensively tested and characterized at Nicosia, Cyprus, during a six-week field campaign in March-April 2015. The field campaign was performed in the framework of the BACCHUS (impact of Biogenic vs. Anthropogenic emissions on Clouds and Climate: towards a Holistic UnderStanding, www.bacchus-env.eu) project. BACCHUS is a European Union's Seventh Framework Programme for Research (FP7) collaborative project of 20 institutes (including CUT and TROPOS), coordinated by ETH Zurich, Switzerland. The BACCHUS Cyprus 2015 field campaign focussed on ground-based and airborne in situ observations of n_{INP} and comparison of these observations with lidar-derived n_{INP} profiles.

The retrieval of the basic lidar products (height profiles of particle backscatter and extinction coefficients) is explained in the next section. In the analysis of lidar data, we need to compute and correct for the contributions of clear air backscattering and extinction (Rayleigh scattering) to the measured total (particle plus Rayleigh) backscatter and extinction coefficients. We downloaded GDAS (Global Data Assimilation System) height profiles of temperature and pressure of the National Weather Service's National Centers for Environmental Prediction (NCEP) for our computations of Rayleigh scattering contributions (NOAA's Air Resources Laboratory ARL, https://www.ready.noaa.gov/gdas1.php). The temperature profiles are also used in the INP parameterizations in Sect. 3.4.

3 Methodology

In this section, the equations for the conversion of the measured optical aerosol properties into the microphysical properties are presented. Figure 1 illustrates the general idea of our approach. Table 2 provides an overview of the different steps of the entire data analysis. All steps 1-6 are explained in detail in the following Sects. 3.1-3.4.

Section 3.1 starts with a brief explanation how we derive and estimate the required height profiles of particle extinction coefficient σ_i for the three aerosol components (index $i =$ d, c, and m), i.e., for desert dust (d), non-desert continental aerosol contributions (c), and marine particles (m). In Sect. 3.2, we present the conversion method applied to obtain the height profiles of the required particle number and surface area concentrations for dry particles of each defined aerosol type (d, c, m) from the lidar-derived profiles of σ_{d}, σ_{c}, and σ_{m}. In Sect. 3.3, we provide a simple parameterization scheme which uses the particle number concentrations $n_{50,i,\mathrm{dry}}$ for $i =$ m and c and $n_{100,\mathrm{d},\mathrm{dry}}$ for desert dust to estimate the CCN-relevant particle number concentration $n_{\mathrm{CCN},ss,i}$. In Sect. 3.4, we present the available INP parameterization schemes (DeMott et al., 2010, 2015; Niemand et al., 2012; Steinke et al., 2015) in which $n_{250,\mathrm{dry}}$ and s_{dry} profiles are input data. Mamouri and Ansmann (2015) already outlined the principle way to obtain dust-related n_{INP} from $n_{250,\mathrm{d},\mathrm{dry}}$ profiles by applying the parameterization of DeMott et al. (2015).

3.1 Aerosol-type-dependent σ profiles from lidar

Steps 1-3 in Table 2 lead to the required height profiles of the particle extinction coefficients σ_{d}, σ_{c}, and σ_{m}. The different retrieval steps are explained in Fig. 2. A lidar observation of a strong Saharan dust outbreak crossing Nicosia during the BACCHUS campaign is presented. This case will be further discussed in Sect. 5.1. As can be seen, the Saharan dust plumes contain (non-desert) aerosol in addition, probably originating from industrial activities in northern Africa (Rodríguez et al., 2011).

In the first step, we determine the height profiles of particle backscatter coefficient β_{p} and particle linear depolarization ratio δ_{p}, here for the transmitted laser wavelength of 532 nm (Fig. 2, left panel). These profiles of β_{p} and δ_{p} allow us to separate the desert dust backscatter coefficient β_{d} and the non-desert backscatter contribution β_{nd} (Fig. 2, center panel). This part of the data analysis is explained in detail by Tesche et al. (2009), Groß et al. (2011), Mamouri et al. (2013), Mamouri and Ansmann (2014), and Nisantzi et al. (2015), and will therefore not be outlined here.

To keep the following steps of the complex data analysis as simple as possible, we concentrate on the aerosol conditions over the polluted European continent and the eastern Mediterranean. We assume that the optical properties over continental sites are related to desert dust and non-desert continental aerosol (urban haze, smoke, soil and road dust, biological particles), only. The impact of marine particles on the overall aerosol optical properties is ignored. Only over the Mediterranean Sea, the North Atlantic, over islands, and in coastal regions we assume that marine particles significantly contribute to the observed optical properties. To keep again the CCN and INP retrievals simple, we ignore a potential marine contribution to aerosol extinction in the free troposphere. This is justified as our numerous lidar observations in remote oceanic areas indicate, as will be discussed in more detail in Sect. 3.4.1. Backward trajectories, AE values from photometer observations, and the usually available retrievals of the particle extinction-to-backscatter ratio (Nisantzi et al., 2015) will support us to estimate the contribution of marine particles in the planetary boundary layer (PBL) to the determined non-desert backscatter coefficient β_{nd}. In Fig. 2, we

assume a small marine contribution of the order of 20% to the non-desert backscatter coefficient.

After the separation of the backscatter contribution, we multiply the three backscatter profiles of $\beta_{\rm d}$, $\beta_{\rm c}$, and $\beta_{\rm m}$ with appropriate lidar ratios of 35-40sr for Middle East dust, 45-55 sr for Saharan dust, 35-75 r for continental non-desert aerosol, and 15-20 sr for marine particles to obtain the σ_i profiles for the three aerosol components (see Fig. 1, step from β to σ, and Fig. 2, right panel). The overall uncertainty in the σ retrieval is estimated to be of the order of 15-25% for desert dust extinction coefficients and 20-40% for the non-desert continental extinction contribution (Tesche et al., 2009; Mamouri et al., 2013; Mamouri and Ansmann, 2014). A significant source of uncertainty is the lidar ratio for continental aerosol which can vary between about 35 sr for almost non-absorbing anthropogenic haze and 75 sr for strongly absorbing biomass burning smoke (Müller et al., 2007; Groß et al., 2013). If a combined Raman/polarization lidar is used, the Raman-lidar derived $\sigma_{\rm p}$ must be in agreement with the sum of the three σ_i profiles (for desert, marine, and non-desert continental aerosol particles) in Fig. 2 (right panel). Strong deviations then usually indicate a wrong estimate of the lidar ratio for continental aerosol pollution, as our experience shows.

3.2 Profiles of $n_{50,\rm dry}$, $n_{100,\rm dry}$, $n_{250,\rm dry}$, and $s_{\rm dry}$ from lidar-derived σ profiles

In the next step (step 4 in Table 2, and the step from σ to n and s in Fig. 1), we derive profiles of the required particle number and surface area concentrations for dry particles from the particle extinction coefficients $\sigma_{\rm d}$, $\sigma_{\rm c}$, and $\sigma_{\rm m}$. Because the observed ambient particle extinction coefficients are related to microphysical properties such as n_{50}, n_{100}, n_{250}, and s at ambient relative humidity conditions, we need to consider water-uptake by hygroscopic particles.

The respective conversion parameters, required to estimate $n_{\rm dry}$ and $s_{\rm dry}$ from the ambient σ values, are obtained from the AERONET correlation study presented in Sect. 4. Regarding water uptake by desert dust, we assume in the correlation studies that desert particles are hydrophobic so that a correction is not necessary. Therefore, we directly used the measured column values of $n_{100,\rm d}$, $n_{250,\rm d}$, and $s_{\rm d}$ in the AERONET correlation study as proxies for $n_{100,\rm d,dry}$, $n_{250,\rm d,dry}$, and $s_{\rm d,dry}$, respectively. As already mentioned in the introduction (Sect. 1) and explained in more detail in Sect. 3.3, $n_{100,\rm d,dry}$ is the appropriate number concentration in the CCN parameterization for desert dust.

For hygroscopic continental aerosol particles, we assume a typical relative humidity of 60% (±20%) for boundary layer aerosols (main reservoir of continental aerosol) as well as for lofted aerosol plumes in the free troposphere. According to 20 years (1995-2015) of radiosonde ascents in Germany (Essen, Munich, and Lindenberg) the mean relative humidity in the boundary layer is 70% (March to October, most AERONET observations are performed during these months) and 75% (January to December, pers. communication, M. Pattantyús-Ábrahám, Meteorological Observatory Hohenpeissenberg). Keeping in mind that lidar observations (and AERONET observations in Sect. 4) are predominantly performed at comparably dry conditions, the assumption of an average relative humidity of around 60% is justified. We assume similar relative humidity conditions in the aerosol layers over Cyprus during times with dominating continental aerosol pollution. The particle radius of continental aerosol particles at 60% relative humidity is about a factor of 1.15 (±0.05) larger than the respective dry particle radius (Skupin et al., 2016). Therefore we use $n_{60,\rm c}$, $n_{290,\rm c}$, and $s_{\rm c}/1.33$ in the following as proxies for $n_{50,\rm c,dry}$, $n_{250,\rm c,dry}$, and $s_{\rm c,dry}$, respectively. As explained in Sect. 2.1, $n_{60,\rm c}$ and $n_{290,\rm c}$ consider all particles with radius >57 nm and > about 290 nm, respectively.

For marine particles we assume a relative humidity of 80% in the water-uptake correction (in the AERONET correlation study). A relative humidity of around 80% is typical for marine boundary layers. At these moist conditions, marine particles are about a factor of 1.6-2 larger than dry marine particles (O'Dowd and de Leeuw, 2007; Zieger et al., 2010, 2013; Zhang et al., 2014). For our study, we use $n_{100,\rm m}$, $n_{500,\rm m}$, and $s_{\rm m}/4$ in the following as proxies for $n_{50,\rm m,dry}$, $n_{250,\rm m,dry}$, and $s_{\rm m,dry}$, assuming that at sea-salt-controlled conditions (sea salt is the most important aerosol type with respect to CCN and INP studies) the particle growth can be as a large as a factor of 2 in radius increase. The comparison of the results obtained with our CCN retrieval for marine particles with in situ observed marine CCNC and particle extinction coefficients (Shinozuka et al., 2015) in Sect. 4 will demonstrate that our selection of $n_{100,\rm m}$ as a basis for the estimation of marine $n_{\rm CCN}$ is appropriate.

In accordance with Shinozuka et al. (2015), we now can make use of the following approach to estimate $n_{50,c,\rm dry}$, $n_{50,m,\rm dry}$, and $n_{100,d,\rm dry}$ from ambient σ_i for the aerosol types $i =$ d, c, and m:

$$n_{100,\rm d,dry}(z) = c_{100,\rm d} \times \sigma_{\rm d}^{x_{\rm d}}(z), \quad (1)$$

$$n_{50,\rm c,dry}(z) = c_{60,\rm c} \times \sigma_{\rm c}^{x_{\rm c}}(z), \quad (2)$$

$$n_{50,\rm m,dry}(z) = c_{100,\rm m} \times \sigma_{\rm m}^{x_{\rm m}}(z) \quad (3)$$

with $n_{100,\rm d,dry}$, $n_{50,\rm c,dry}$, and $n_{50,\rm m,dry}$ in $\rm cm^{-3}$, the conversion factor $c_{100,\rm d}$, $c_{60,\rm c}$, and $c_{100,\rm m}$ in $\rm cm^{-3}$ for the ambient particle extinction coefficient $\sigma_i = 1\,\rm Mm^{-1}$, the ambient particle extinction coefficient σ_i in $\rm Mm^{-1}$, and the aerosol extinction exponent x_i. Equations (1)-(3) assume a linear correlation of $\log n_{100,\rm d}$ with $\log\sigma_{\rm d}$, $\log n_{60,\rm c}$ with $\log\sigma_{\rm c}$, and $\log n_{100,\rm m}$ with $\log\sigma_{\rm m}$. Values for $c_{100,\rm d}$, $c_{60,\rm c}$, $c_{100,\rm m}$, and x_i are given in Table 3 for all three laser wavelengths. Determination of the specific parameters $c_{100,\rm d}$, $c_{60,\rm c}$, and $c_{100,\rm m}$ and x_i is explained in Sect. 4 (AERONET correlation study).

$n_{250,i,\rm dry}$ for aerosol type i is related to the corresponding

particle extinction coefficient σ_i as follows:

$$n_{250,\mathrm{d,dry}}(z) = c_{250,\mathrm{d}} \times \sigma_{\mathrm{d}}(z), \quad (4)$$

$$n_{250,\mathrm{c,dry}}(z) = c_{290,\mathrm{c}} \times \sigma_{\mathrm{c}}(z), \quad (5)$$

$$n_{250,\mathrm{m,dry}}(z) = c_{500,\mathrm{m}} \times \sigma_{\mathrm{m}}(z) \quad (6)$$

with $n_{250,i,\mathrm{dry}}$ in cm^{-3}, the conversion factors $c_{250,\mathrm{d}}$, $c_{290,\mathrm{c}}$, and $c_{500,\mathrm{m}}$ in $\mathrm{cm}^{-3}\mathrm{Mm}$, and the particle extinction coefficient σ_i in Mm^{-1}. Equations (4)-(6) assume a linear relationship between the large particle fraction n_{250} and σ_{d}, n_{290} and σ_{c}, and n_{500} and σ_{m}. Again, the conversion factors $c_{250,\mathrm{d}}$, $c_{290,\mathrm{c}}$, and $c_{500,\mathrm{m}}$ are listed in Table 3. They are obtained from the correlation analysis in Sect. 4.

Finally, we obtain the particle surface area concentration s_{dry} for aerosol type i from

$$s_{\mathrm{d,dry}}(z) = c_{\mathrm{s,d}} \times \sigma_{\mathrm{d}}(z), \quad (7)$$

$$s_{\mathrm{c,dry}}(z) = c_{\mathrm{s,c}}/1.33 \times \sigma_{\mathrm{c}}(z), \quad (8)$$

$$s_{\mathrm{m,dry}}(z) = c_{\mathrm{s,m}}/4 \times \sigma_{\mathrm{m}}(z) \quad (9)$$

with $s_{i,\mathrm{dry}}$ in $\mathrm{m}^2\,\mathrm{cm}^{-3}$ and the conversion factor $c_{\mathrm{s},i}$ in $\mathrm{m}^2\,\mathrm{cm}^{-3}\mathrm{Mm}$. Again, a linear relationship between particle surface area s_i and particle extinction coefficient σ_i is assumed. The $c_{\mathrm{s},i}$ values are listed in Table 3. The overall uncertainties in all retrievals will be discussed in Sect. 4.4. Standard deviations of all conversion parameters in Table 3 are the basic information in the uncertainty analysis.

3.3 Profiles of $n_{\mathrm{CCN},ss}$ from $n_{50,\mathrm{dry}}$ and $n_{100,\mathrm{dry}}$ profiles

In the next step (step 5 in Table 2 and in Fig. 1, the step from $n_{50,dry}$ and $n_{100,dry}$ to n_{CCN}), we estimate the profiles of CCN-relevant particle number concentrations. The CCN parameterization is a crucial task. Therefore only the basic approach is presented here. The ability of aerosol particles to serve as CCN is a function of their size, chemical composition, and the level of supersaturation in the ambient cloud layer. The supersaturation ss depends on the updraft velocities and typically is in the range of $ss = 0.1\%$ to 1%. The higher the supersaturation, the smaller the particles that can be activated, and thus the higher the number concentration of potential CCN. We will restrict our CCN parameterization here to low supersaturation of 0.1-0.2%. The CCN number concentration can be easily a factor of 2-3 higher when the updraft speeds causes conditions with supersaturation of 0.4-1%.

In the case of desert dust, the situation is even more complex (Kumar et al., 2009, 2011; Koehler et al., 2009). During emission, desert dust particles may contain negligible amounts of soluble material. They are typically hydrophobic. During long-range transport, dust particles undergo atmospheric processing and soluble species may form on the particle surfaces. In this way, the ability of desert dust particles to serve as CCN may be significantly improved. A factor 2 or even more particles may be activated. Observations by Shinozuka et al. (2015) and our own SALTRACE observations (CCN number concentrations from airborne in situ observations and particle extinction coefficients from ground-based lidar) however suggest that the soluble fraction must be small, at least for Saharan dust after the long-range transport over 5000-8000 km, so that $n_{100,\mathrm{d,dry}}$ is a good proxy for the particle number concentration of the desert-dust-related CCN reservoir here. This aspect will be further discussed in Sect. 4.

We estimate $n_{\mathrm{CCN},ss,i}$ now in the following way:

$$n_{\mathrm{CCN},ss,\mathrm{d}}(z) = f_{ss,\mathrm{d}} \times n_{100,\mathrm{d,dry}}(z), \quad (10)$$

$$n_{\mathrm{CCN},ss,\mathrm{c}}(z) = f_{ss,\mathrm{c}} \times n_{50,\mathrm{c,dry}}(z), \quad (11)$$

$$n_{\mathrm{CCN},ss,\mathrm{m}}(z) = f_{ss,\mathrm{m}} \times n_{50,\mathrm{m,dry}}(z), \quad (12)$$

with $f_{ss,i} = 1.0$ for $ss = 0.15\%$. According to the literature, non-desert aerosol particles with dry particle radius of about > 40 nm (at $ss = 0.25\%$) and > 30 nm (at $ss = 0.4\%$) form the reservoir of potential CCN (Quinn et al., 2008; Rose et al., 2010; Deng et al., 2011; Ditas et al., 2012; Siebert et al., 2013; Henning et al., 2014). This was found from a variety of studies conducted in very different regions of the world and for very different aerosol mixtures. Only for supersaturation values of about 0.2% and lower, $n_{50,\mathrm{dry}}$ seems to represent the particle number concentration of the CCN reservoir. By inspection of the size distributions for pure marine aerosols (Bates et al., 2000), continental pollution aerosol (Beddows et al., 2014) and our own Leipzig city size distributions (measured at TROPOS throughout the year 2008), we found $n_{30,\mathrm{dry}}/n_{50,\mathrm{dry}}$ ratios on the order of 1.7 ($\pm$0.8) and $n_{40,\mathrm{dry}}/n_{50,\mathrm{dry}}$ of about 1.35 ($\pm$0.7). These values may be used as the enhancement factor $f_{ss,i}$ in Eqs. (10)-(12), i.e., $f_{ss=0.25\%,i}$ =1.35 and $f_{ss=0.4\%,i}$ =1.70. Ji and Shaw (1998) found for pure ammonium sulfate in laboratory studies enhancement factors of 1.26 ($ss = 0.25\%$) and 1.46 ($ss = 0.4\%$). Shinozuka et al. (2015) assumes an increase of n_{CCN} by a factor of 2 when the supersaturation increases from 0.2 to 0.4%. Hiranuma et al. (2011) however also mentioned that natural aerosols show a much more complex behavior regarding these enhancement factors than discussed here.

In the case of desert dust, cloud droplet activation may include particles with dry radius as low as 50 nm at supersaturation of 0.15-0.2%, when the particles are coated with soluble material. According to the AERONET size distributions, the number concentration $n_{50,\mathrm{dry}}$ is roughly a factor of 4 higher than $n_{100,\mathrm{dry}}$. All these uncertainties lead to the conclusion of Shinozuka et al. (2015) that the uncertainty range for $n_{\mathrm{CCN},ss,i}$ is best described by a factor of 3 around the derived solutions. By using $n_{60,\mathrm{c}}$, $n_{100,\mathrm{m}}$, and $n_{100,\mathrm{d}}$ as proxies for $n_{50,\mathrm{c,dry}}$, $n_{50,\mathrm{m,dry}}$, and $n_{100,\mathrm{d,dry}}$ in Eqs. (10)-(12), the $n_{\mathrm{CCN},ss=0.15\%}$ values presented in Sects. 4 and 5 may be therefore interpreted as the mimimum values of the possible solution space for $n_{\mathrm{CCN},ss}$.

3.4 Profiles of n_{INP} from $n_{250,\mathrm{dry}}$ and s_{dry} profiles

The final step of the retrieval (step 6 in Table 2, and in Fig. 1, the step from $n_{250,i,\mathrm{dry}}$ and s_{dry} to $n_{\mathrm{INP},i}$) leads to the estimation of the INP number concentration profiles. Different parameterizations can be used based on $n_{250,\mathrm{dry}}$ (DeMott et al., 2010, 2015) or s_{dry} profiles (Niemand et al., 2012; Steinke et al., 2015).

3.4.1 Estimation of n_{INP} from $n_{250,\mathrm{dry}}$

The INP parameterizations introduced by DeMott et al. (2010, 2015) hold for $n_{250,\mathrm{dry}}(p_0,T_0)$ and thus standard (std) pressure ($p_0 = 1013\,\mathrm{hPa}$) and temperature ($T_0 = 273.16\,\mathrm{K}$) conditions (see Eqs. 13 and 14). Therefore, we have to convert each profile value $n_{250,\mathrm{dry}}(p_z,\,T_z)$ from ambient pressure p_z and temperature T_z at height z to $n_{250,\mathrm{dry}}(p_0,T_0)$ by using the factor $(T_z p_0)/(T_0 p_z)$.

DeMott et al. (2010) introduced a so-called global INP parameterization which is based on nine field campaigns conducted in Colorado (4 campaigns), eastern Canada (2 campaigns), Amazonia, Alaska, and in the Pacific Basin. This INP characterization scheme is, to our opinion, suitable for an INP parameterization of non-desert continental aerosols (for mixtures of anthropogenic haze, biomass burning smoke, biological particles, soil and road dust):

$$n_{\mathrm{INP,c}}(p_0,T_0,T_z) = a_1(273.16-T_z)^{b_1} \times n_{250,\mathrm{c,dry}}(p_0,T_0)^{[c_1(273.16-T_z)+d_1]} \quad (13)$$

with $n_{250,\mathrm{c,dry}}$ in $\mathrm{std\,cm^{-3}}$, $n_{\mathrm{INP,c}}$ in $\mathrm{std\,L^{-1}}$, $a_1 = 0.0000594$, $b_1 = 3.33$, $c_1 = 0.0265$, $d_1 = 0.0033$, and temperature $T(z)$ in K (and $< 273.16\,\mathrm{K}$). Note that the values of a_1,b_1,c_1 and d_1 given in Mamouri and Ansmann (2015) are erroneous. However, all computations presented in that article were performed with the correct values listed here.

Finally, we transfer the obtained values of $n_{\mathrm{INP,c}}(p_0,T_0,T_z)$ to the ones for ambient pressure and temperature conditions, $n_{\mathrm{INP,c}}(p_z,T_z)$, by multiplying $n_{\mathrm{INP,c}}(p_0,T_0,T_z)$ with the factor $(T_0 p_z)/(T_z p_0)$.

It should be emphasized that this INP parameterization shows an uncertainty in the range of a factor of 5-10 as recent observation indicate (McCluskey et al., 2014; Mason et al., 2015; Taylor et al., 2016a,b). The most obvious reason for the remaining uncertainty is that the specific aerosol composition, i.e., the mixture of aerosol types (the exact amount of pollen, dust, soot, organic material, and sulfates) during an actual measurement case is not known. Strong differences in the INP efficacy of different aerosol types is found in laboratory studies (see review of Murray et al. (2012)). Furthermore, observations also indicate that particles with radii <250 nm may be activated as well (Mason et al., 2016). The size effect was found to increase with decreasing temperature. Nevertheless, we use this schemes for continental aerosol mixtures (by excluding explicitly desert dust) because it explains many of the details of the found relationship between the observed fractions of ice-containing clouds and cloud top temperature of altocumulus layers which formed over the European continent in aged aerosol mixtures. This INP parameterization especially predicts significant heterogeneous ice nucleation already at high temperatures of -5 to $-15^{\circ}\mathrm{C}$ as observed (Seifert et al., 2010; Kanitz et al., 2013).

The INP parameterization scheme for mineral dust of DeMott et al. (2015) is used here explicitly for desert dust:

$$n_{\mathrm{INP,d}}(p_0,T_0,T_z) = f_{\mathrm{d}} n_{250,\mathrm{d,dry}}(p_0,T_0)^{[a_2(273.16-T_z)+b_2]} \times \exp[c_2(273.16-T_z)+d_2] \quad (14)$$

with the so-called atmospheric correction factor $f_{\mathrm{d}} = 3$, and the coefficients $a_2 = 0.0$, $b_2 = 1.25$, $c_2 = 0.46$, and $d_2 = -11.6$. Again, to obtain the n_{INP} profile for ambient temperature and pressure conditions, we have to transfer the obtained values of $n_{\mathrm{INP,d}}(p_0,T_0,T_z)$ to the ones for ambient pressure and temperature conditions in the same way as described above for $n_{\mathrm{INP,c}}(p_z,T_z)$, namely by multiplying $n_{\mathrm{INP,d}}(p_0,T_0,T_z)$ with the factor $(T_0 p_z)/(T_z p_0)$.

According to DeMott et al. (2015), Eqs. (13) and (14) can be used to estimate n_{INP} for immersion freezing processes. The formulas are applicable to the temperature range from -9 to $-35\,^{\circ}\mathrm{C}$ (Eq. 13) and -21 to $-35\,^{\circ}\mathrm{C}$ (Eq. 14). In Sect. 5 (lidar case studies), we use these immersion-freezing-based parameterizations for higher as well as lower temperatures. According to Wex et al. (2014) ice nucleation for anthropogenic particles (with an insoluble part) and coated mineral dust particles (coated with natural and/or anthropogenic soluble material) can be described as immersion freezing as well, even at temperatures $< -35\,^{\circ}\mathrm{C}$. Above the deliquescence relative humidity, additional water is added to the coating and a solution shell forms around the insoluble part of the particles, causing them to nucleate ice from concentrated solutions via the immersion freezing pathway, taking a freezing point depression into account.

Regarding the uncertainties in the INP computation, we assume that Eq. (14) allows a prediction of dust n_{INP} within an uncertainty range of a factor of 2-5 (DeMott et al., 2015; Schrod et al., 2015). An overview of all uncertainties in the basic lidar-derived particle optical properties, the retrieved microphysical aerosol properties, and the finally estimated $n_{\mathrm{INP},i}$ values is given in Sect. 4.4.

Recently, DeMott et al. (2016) compared the potency of marine and continental INPs. By comparing laboratory studies and field observations it was found that for typical marine (sea salt aerosol) and continental aerosol conditions characterized by ambient particle extinction coefficients of 50-100 $\mathrm{Mm^{-1}}$ at 500 nm wavelength, the marine INP number concentration was lower by about three orders of magnitude than the continental INP number concentration. Compared to terrestrial particles, sea salt particles are obviously bad INPs (efficacy is a factor of 300-500 lower) which is in agreement with mixed-phase cloud observations in the northern midlatitudes (high amount of terrestrial particles) and in the

southern Ocean (Punta Arenas, Chile, very low amount of terrestrial particles) (Seifert et al., 2010; Kanitz et al., 2011). However, the temperature dependence of heterogeneous ice formation caused by marine and terrestrial particles (as given by Eq. 13) was found to be similar (DeMott et al., 2016). Therefore, in order to roughly estimate marine $n_{\mathrm{INP,m}}$ we simply use Eq. (13) with $n_{\mathrm{250,m,dry}}$ (after Eq. 6) as input and divide the resulting n_{INP} value by 350 (DeMott et al., 2016).

In the estimation of actual marine INP number concentrations at given environmental conditions (mixture of marine and terrestrial aerosols) one should mentioned again that the polarization lidar technique allows us to separate dust from non-dust aerosol components, but not a further separation of marine from continental aerosol pollution. We must therefore estimate the impact of marine particles on the non-desert aerosol extinction coefficient. As stated in Sect. 3.1, over the oceans, we can assume that the extinction coefficient in the PBL is widely determined by marine particles. In continental outflow regimes and at coastal sides (because of sea breeze effects) we must estimate the contribution by continental particle scattering and absorption to the overall aerosol extinction coefficient in the PBL. We may use the AE information from AERONET observations or multiwavelength lidar observations to estimate the contributions by marine and continental particles to the observed overall non-desert extinction coefficient.

As stated in Sect. 3.1, we ignore a marine contribution of σ_{m} to the particle extinction coefficient in the free troposphere, and therefore a marine contribution to the CCN and INP reservoirs (n_{CCN}, n_{INP}) in the free troposphere. This is corroborated by our lidar observation at Punta Arenas, Chile, Cape Town, South Africa, aboard the R/V Polarstern, and many Polly lidar sites around the globe (Kanitz et al., 2013; Seifert et al., 2015; Baars et al., 2012, 2015). We conclude from these lidar observations that the marine extinction coefficient σ_{m} is <1-2 Mm^{-1} for free-tropospheric heights <3-5 km, and of the order of 0.01-0.2 Mm^{-1} for heights >5 km. Only by strong updrafts below cumulus towers with cloud base in the marine PBL, a large amount of marine particles over oceanic sites may be injected into the free troposphere and may trigger strong heterogeneous ice formation when the air parcels ascent to heights with temperatures below -25°C. For typical marine ambient particle extinction coefficients of 50-100 Mm^{-1} in the marine PBL, we obtain an estimate of roughly 5-10 INP per m^3 at -25 °C. At free tropospheric aerosol background conditions with marine particle extinction coefficients of the order of 0.1-1 Mm^{-1}, $n_{\mathrm{INP,m}}$ is in the range from 0.01-0.1 m^{-3} at temperatures of -25°C according to the study of DeMott et al. (2016), and thus 4-5 orders of magnitude lower than $n_{\mathrm{INP,d}}$ in our dust outbreak case study at -25°C (at 6.5 km height) presented in Sect. 5.1.

3.4.2 Estimation of n_{INP} from s_{dry}

$n_{\mathrm{INP,d}}$ profiles can also be estimated from the s_{d} profiles. An immersion-freezing INP parameterization is provided by Niemand et al. (2012):

$$n_{\mathrm{INP,d}}(T_z) = 1000 \times s_{\mathrm{d,dry}}(z) \times \eta_{\mathrm{im}}(T_z), \quad (15)$$

$$\eta_{\mathrm{im}}(T_z) = \exp[-0.517(T_z - 273.16) + 8.934] \quad (16)$$

with $n_{\mathrm{INP,d}}$ in L^{-1}, $s_{\mathrm{d,dry}}$ in $\mathrm{m}^2\,\mathrm{cm}^{-3}$ (so that a multiplication by 1000 is needed to obtain s in $\mathrm{m}^2\,\mathrm{L}^{-1}$), and η_{im} in m^{-2}. The $n_{\mathrm{INP,d}}$ profile holds for temperatures from 237–261 K (−12 to −37 °C).

Steinke et al. (2015) provides a deposition-freezing parameterization:

$$n_{\mathrm{INP,d}}(T_z) = 1000 \times s_{\mathrm{d,dry}}(z) \times \eta_{\mathrm{dep}}(T_z), \quad (17)$$

$$\eta_{\mathrm{dep}}(T_z) = 1.88 \times 10^5 \times \exp(0.2659\chi(T_z)), \quad (18)$$

$$\chi(T_z) = -(T_z - 273.16) + (ss_{\mathrm{ICE}} - 1) \times 100 \quad (19)$$

with ice supersaturation of ss_{ICE}. We assume a constant, but reasonable value of 1.15 for ss_{ICE} indicating frequently occurring moderate supersaturation conditions in ice clouds (Comstock et al., 2008). The $n_{\mathrm{INP,d}}$ profile holds for temperatures from 220–253 K (−20 to −53 °C). This deposition freezing parameterization, however, is based on laboratory studies of heterogeneous ice nucleation on artificially produced mineral dust particles (Arizona test dust) which usually show an enhanced freezing efficacy compared to natural desert dust aerosols.

4 AERONET correlation study

Of key importance for the entire retrieval of cloud-relevant microphysical aerosol parameters from lidar-derived particle extinction coefficient profiles at ambient conditions are trustworthy conversion parameters $c_{\mathrm{60,c}}$, $c_{\mathrm{100,d}}$, $c_{\mathrm{100,m}}$, $c_{\mathrm{250,d}}$, $c_{\mathrm{290,c}}$, $c_{\mathrm{500,m}}$, $c_{\mathrm{s},i}$, and exponents x_i as required to solve Eqs. (1)–(9). These conversion parameters are derived from the long-term AERONET observations at Leipzig and Limassol (for northern and southern European continental aerosol mixtures), at Ragged Point (for pure marine conditions), and the short-term dust-related field campaigns in Morocco, Cabo Verde, and Barbados (for pure desert dust scenarios, see Table 1). The main results of the AERONET data analysis are presented and discussed in this section.

We performed the AERONET correlation study separately for all three laser wavelengths, but show the results for the mostly used lidar wavelength of 532 nm, only. To facilitate our studies and to be in consistency with the work of Shinozuka et al. (2015), who investigated the correlation between CCNC and σ at 500 nm, we replaced all column integrals, i.e., AOTs and the column values of n and s by respective volume-related values. For this, we introduced a normalizing, arbitrarily selected vertical column height of 1000 m

and divided all basic AERONET observational data points by 1000 m. An example of the transformation is illustrated in Fig. 3 for the Leipzig observation of the column-integrated n_{250} and AOT at 532 nm. The volume-related values can be interpreted as the vertical averages of n, s, and σ in the assumed 1000 m deep column. It should be mentioned that the selected column height has no impact on the data analysis, but is set to a realistic value so that the range of σ, typically measured with lidar for a given site, is covered.

4.1 Leipzig and Limassol long-term observations of mixed aerosols

A total number of 48 474 and 34 982 sun/sky photometer observation (level 1.5) were taken at Limassol and Leipzig, respectively, during the 2011–2015 (Limassol) and 2001-2015 (Leipzig) time periods. 4190 and 4651 of these measurements at Limassol and Leipzig could be used to derive particle size distributions and thus column values of n and s. 1745 Limassol and 2157 Leipzig quality-assured level-2.0 data sets were finally available for our study. The observed correlations of n_{60}, n_{290}, and $s/1.33$ vs 532 nm σ for pollution-dominated scenarios (Ångström exponents AE > 1.4 and > 1.6) and of n_{100}, n_{250}, and s for the desert-dust-dominated cases (AE < 0.7 and < 0.5) are shown in Figs. 4 and 5. The conversion parameters derived from the correlation analysis are given in Table 3 and used in Eqs. (1)–(9).

As shown in Figs. 4 and 5, at both sites a large variability in the aerosol conditions is observed. Limassol in the eastern Mediterranean experiences complex aerosol conditions almost every day. This Middle East (Eastern Mediterranean) station is influenced by frequent dust outbreaks from the Sahara and the Middle East deserts (Nisantzi et al., 2015), biomass burning smoke and fire-induced soil dust injections (Nisantzi et al., 2014) from Turkey, the Black Sea area, and European regions further to the north, and anthropogenic haze from eastern, southeastern and southern Europe, northern Africa, and western Asia. Marine particles form the background aerosol at Limassol at the south coast of Cyprus. In contrast, the central European AERONET station of Leipzig is heavily influenced by fresh and aged anthropogenic pollution, which dominates the boundary layer aerosol (Mattis et al., 2004; Wandinger et al., 2004). A few Saharan dust outbreaks towards central Europe (Ansmann et al., 2003; Papayannis et al., 2008) and long-range transport of biomass burning aerosol and anthropogenic haze from southern Europe and North America determine the aerosol conditions in the free troposphere (Mattis et al., 2008). On average, the free-tropospheric AOT contributes 20 % to the overall AOT (Mattis et al., 2004). The impact of marine aerosol on the Leipzig observations is negligible.

The top panels in Figs. 4 and 5 nicely show that the Limassol and Leipzig AERONET observations are complementary from the statistics point of view. Much more cases with a strong desert dust impact are measured at Limassol (133 cases with AE<0.5 within 4 years) than at Leipzig (only 33 dust cases in 14 years). The opposite is true for well-mixed anthropogenic haze (with AE>1.6). About 1000 observations are available for Leipzig covering a broad range of particle extinction values from 40-700 Mm^{-1}, whereas at Limassol homogeneous haze/smoke situations are less frequent (421 observations with AE>1.6) and the ambient extinction values cover a range from 30-400 Mm^{-1} only. We used AE calculated from the AOT values from 440 to 870 nm here to filter out dust-dominated and haze-dominated aerosol observations.

The found scatter in the correlations of n_{60}, n_{100}, n_{250}, n_{290}, and s with σ in Figs. 4 and 5 is caused by many reasons. First of all, different particle size distributions (leading to different n and s values) can produce the same σ value. The optical efficiency (optical cross section divided by the geometrical cross section $s/4$) of a given log-normal aerosol size distribution can easily vary between 0.3 and 3 as a function of a shifting mode radius of the fine-mode particle spectrum towards larger or smaller sizes without leading to significant changes in the n and s values. The particle optical effects depend on ambient relative humidity (significant water up-take by particles occurs when the relative humidity in the vertical column exceeds 75-80%) so that large changes in σ (within a factor of 1.5–2.5) may be correlated with comparably small changes in n_{60}, n_{100}, n_{250}, n_{290}, and s. The aerosol mixtures (or the overall chemical composition of the particles including the type-dependent water uptake and growth effects) may be different for relatively clean aerosol conditions (low σ values) and scenarios with heavy pollution or dust outbreaks (high σ values). All this systematically influence the correlation features. The discussed uncertainties in the retrieval of the particle size distribution, n, and s (case by case, Sect. 2.1) as quantified by Dubovik et al. (2000) also contribute to the observed variability in the correlations.

As recommended by Shinozuka et al. (2015), we applied the regression analysis to the logn_{60}-logσ and logn_{100}-logσ data fields (top panels in Figs. 4 and 5). The regression lines in the figures go through the geometric averages of n_{100} and n_{60} for the average σ value. The slope of the regression line is the extinction exponent x in Eqs. (1) and (2). The obtained numbers for $x_{\rm d}$, $x_{\rm c}$, $c_{100,\rm d}$, and $c_{60,\rm c}$ of the log-log regression analysis are given in Table 3 (Cyprus and Germany observations). The standard deviations (root mean square values) of the regressions analysis are mostly 0.15–0.25 in the log scale and thus indicate overall uncertainties within a factor of 1.4–1.8 for $n_{60,\rm c}$ and $n_{100,\rm d}$ when estimated from σ. Taking an additional uncertainty in the water-uptake correction into account, we estimate that $n_{100,\rm d,dry}$ (Eq. 1) and $n_{50,\rm c,dry}$ (Eq. 2) can be estimated with an uncertainty of a factor of 1.5-2.

We compared our results with respective ones presented by Shinozuka et al. (2015) for likewise rural and background sites (Southern Great Plains, Oklahoma, Cape Cod, Massachusetts, Black Forest, Germany). In these measurements,

the dry extinction coefficients for 500 nm wavelengths mainly ranged from 5-100 Mm^{-1}. The comparison reveals that the Limassol and Leipzig AERONET data sets clearly represent highly polluted urban conditions. Our observations considered in Figs. 4 and 5 cover an AE range from 1.6-2.2 and thus indicate the strong impact of fine-mode aerosol in these measurements. By using the Leipzig conversion parameters in Table 3 ($c_{60,\mathrm{c}} = 25.3\ \mathrm{cm}^{-3}$ at $\sigma_\mathrm{c} = 1\ \mathrm{Mm}^{-1}$, $x_\mathrm{c} = 0.94$) we obtain $n_\mathrm{CCN} \approx 1000\,\mathrm{cm}^{-3}$ for an ambient extinction value of $\sigma_\mathrm{c} = 50\ \mathrm{Mm}^{-1}$ in Eq. (2) and when inserting the resulting $n_{50,\mathrm{c,dry}}$ in Eq. (11). For Limassol we get even higher CCN-relevant values ($n_\mathrm{CCN} \approx 2000\,\mathrm{cm}^{-3}$ for $\sigma_\mathrm{c} = 50\ \mathrm{Mm}^{-1}$). Similar values are obtained from horizontal long-path particle extinction measurements at ambient conditions at TROPOS, Leipzig, (Skupin et al., 2014, 2016) and accompanying continuous dry-particle size distribution observations (pers. communication, Annett Skupin).

The measurements of Shinozuka et al. (2015) at more rural and background sites indicate n_CCN of 400-500 cm^{-3} (Southern Great Plains), 350-400 cm^{-3} (Black Forest), and around 700 cm^{-3} in the case of Cape Cod at the Atlantic Ocean in the northeastern United States for ambient extinction coefficients of 50 Mm^{-1} at 500 nm and for the AE class from 1.5-1.7 (indicating less fine-mode dominated aerosols compared to the Limassol and Leipzig aerosol conditions). To compare our data (for supersaturations of 0.15% and ambient instead of dry particle extinction coefficients), we divided the CCNC numbers of Shinozuka et al. (2015), measured at supersaturations around 0.4%, by a factor of 2, assuming that the resulting numbers then represent CCNC values for $ss = 0.15\%$, and we multiplied the dry extinction coefficients with a factor of 1.4 to obtain ambient extinction coefficients, assuming relative humidities of 60-70% prevail also in the aerosol layers over Oklahoma, Massachusetts, and the Black Forest in southern Germany.

In this context, it is also noteworthy to mention that Liu and Li (2014) showed that the product of $\sigma \times \mathrm{AE}$ (denoted as Aerosol Index AI, introduced by Nakajima et al., 2001) provides a better correlation with n_CCN than n_CCN with σ. By using AI instead of σ in the correlation, Liu and Li (2014) consider information on the aerosol type and the related size distribution (high AI for fine-mode-dominated aerosol, low AI for coarse-mode-dominated aerosol conditions). Similarly, Shinozuka et al. (2015) separated the observations in classes with AE from 1.5–1.7 and from 0.3–0.5, and derived AE-dependent parameterizations to obtain estimates of n_CCN from σ observations. In contrast to these approaches, the advantage of our lidar technique is that we separate the different aerosol types by means of the polarization lidar technique first, i.e., before we apply our parameterization and conversion procedures to estimate the microphysical and cloud-relevant aerosol parameters for each aerosol type separately.

A complex regression data analysis as in the top panels of Figs. 4 and 5 is not needed in the study of the n_{250}–σ, n_{290}–σ, and s–σ relationships. We can assume simple linear relationships because the optical effects of the aerosol mixtures depend approximately linearly on s, n_{250}, and n_{290}. For all individual, single AERONET observations (belonging to the separate data sets for $\mathrm{AE} > 1.6$ and $\mathrm{AE} < 0.5$) we calculated the n_{250}/σ, n_{290}/σ, and s/σ ratios for all three laser wavelengths. In Figs. 4 and 5, the geometrical averages of these ratios (for 532 nm σ) define the slopes of the shown straight lines. Shown are both slopes for the fine-mode (AE>1.6) and coarse-mode (AE<0.5) classes. The mean values of n_{250}/σ, n_{290}/σ, and s/σ for each aerosol subdata set ($\mathrm{AE} < 0.5$, $\mathrm{AE} > 1.6$) are used as $c_{250,\mathrm{d}}$, $c_{290,\mathrm{c}}$, $c_{\mathrm{s,d}}$ and $c_{\mathrm{s,c}}$, respectively, in Eqs. (4), (5), (7), and (8). All Leipzig and Limassol values of $c_{250,\mathrm{d}}$, $c_{290,\mathrm{c}}$, $c_{\mathrm{s,d}}$ and $c_{\mathrm{s,c}}/1.33$ together with SD (obtained from the averaging procedure) are given in Table 3.

Our results are in good agreement with combined airborne in situ observations of particle number concentration $n_{150,\mathrm{dry}}$ (particles with dry radius >150 nm) and lidar-derived particle backscatter coefficients at 532 nm in southern Japan at marine, moderately polluted summer conditions (Sakai et al., 2013). Measurements were performed between 500 m and 5 km height and were influenced by long-range transport of pollution and dust from eastern Asia. By assuming a particle extinction-to-backscatter ratio of 50 sr (typical for a mixture of aged pollution and dust), the conversion factor for the measurements in southern Japan is $c_{150} \approx 1.0\ \mathrm{Mm\,cm}^{-3}$ (AE ranged from about 0.3 to 1.0). Our AERONET study indicates for dusty environments that $n_{150,\mathrm{dry}}$ is a factor of roughly 5 higher than $n_{250,\mathrm{dry}}$. Consequently, our conversion factor $c_{250} \approx 0.2\ \mathrm{Mm\,cm}^{-3}$ is five times lower than the c_{150} value.

Our results are also in good agreement with respective model studies of s for various aerosol types conducted by Barnaba and Gobbi (2001, 2002). According to Barnaba and Gobbi (2001), the s–σ ratio for 500–550 nm for example should be in the range of 2–4 for particle size distributions with strong coarse mode. Kolgotin et al. (2015) found a value of 1.6 ($\pm 20\,\%$) for the s/σ ratio at the 355 nm wavelength. In their simulations, they considered monomodal log-normal size distributions with mean radius from 20 to 300 nm. We conclude from their study that the s/σ values are in the range from 2.4–3 for 532 nm for haze and dust conditions.

The scatter of the individual observations for the typical range of σ from 50–400 Mm^{-1} provides insight into the uncertainty in the retrieval of the particle number concentrations and surface area concentrations from the measured particle extinction coefficients. The respective standard deviations of $c_{250,\mathrm{d}}$, $c_{290,\mathrm{c}}$, $c_{\mathrm{s,d}}$, and $c_{\mathrm{s,c}}$ in Table 3 are used in the error analysis in Sects. 4.4. The standard deviations roughly indicate that conversions of σ into $n_{250,\mathrm{d}}$, $n_{290,\mathrm{c}}$, and s is possible with a relative error of 20–30 %.

4.2 Field campaign data sets for pure dust conditions

Unique combined AERONET photometer and multiwavelength lidar observations are available for pure Saharan dust conditions, sampled during several field campaigns in southeastern Morocco (SAMUM-1), close to the dust source at a minimum influence by marine particles and anthropogenic pollution, at Cape Verde (SAMUM-2) during a heavy dust outbreak from 28–30 January 2008, and at Barbados (SALTRACE-1 and 3, lofted dust plumes during the summer months) in the long-range dust transport regime, 5000–8000 km west of the Saharan dust sources (see Table 1).

From all the SAMUM and SALTRACE observations we were able to carefully select 125 cases with dominant dust conditions (indicated by AE values <0.2). For all these data sets, detailed lidar observations of dust layering (layer structures, base and top heights of main dust layers) (Tesche et al., 2009, 2011; Haarig et al., 2015; Groß et al., 2015) are available so that mean dust extinction coefficients and mean values of particle number and surface area concentrations could be calculated for the observed dust layers by combining the AERONET column observations and the layer depth information from the lidar. The results shown in Fig. 6 are based on these dust layer mean values. We also checked all AERONET measurements carefully regarding cloud contamination (subvisible and thin cirrus) by means of the lidar observations. Furthermore, we launched 1-3 radiosondes per day. The relative humidity in the dust layers over Cabo Verde and Barbados was always $< 50\,\%$.

Unfortunately, problems with the AERONET 340 nm channel in Morocco and Barbados (in 2014, SALTRACE-3) prohibit the retrieval of conversion parameters at 355 nm. So, we present the conversion parameters at 380 nm in Table 3 which fairly well represent the parameters for 355 nm in the case mineral dust. Furthermore, the Morocco size distributions are not trustworthy for small particles (sometimes rather high peaks in number concentrations occurred for size bins from 50 to 112 nm radius). The reasons may be related to the missing 340 nm channel and to the fact that the occurrence of very large particles with radius >15 μm at a site close to the desert dust sources can never be excluded (Müller et al., 2010). The AERONET size distribution retrieval, however, considers particles with radius up to 15 μm, only. We therefore did not consider the Morocco AERONET observations in the correlation analysis for $n_{100,\mathrm{d}}$ and s_d with σ_d in Fig. 6. The desert dust conversion factors in Table 3 are exclusively derived from the Cabo Verde and Barbados observational data.

The results of the correlation analysis in Fig. 6 (for 532 nm) are given in the same way as for the multi-year Leipzig and Limassol data in Figs. 4 and 5. As can be seen, there is much less scatter in the SAMUM and SALTRACE dust observations compared to the observations for the aerosol mixtures over the urban sites of Leipzig and Limassol.

The CCN-relevant correlation study ($n_{100,\mathrm{d}}$ vs σ_d) is in good agreement with field observations of Shinozuka et al. (2015) at the dusty site of Niamey (Niger, western Africa, south of the Sahara). The simultaneous observation of CCNC and dry extinction coefficients observations (for the class with AE from 0.3-0.5) yield $n_\mathrm{CCN} \approx 110 - 120\,\mathrm{cm}^{-3}$ for a supersaturation level of 0.2% and an (ambient) dust extinction coefficient of $\sigma_\mathrm{d} = 50$ Mm^{-1}. Our parameterization yields $n_\mathrm{CCN} \approx 100\,\mathrm{cm}^{-3}$ for $\sigma_\mathrm{d} = 50$ Mm^{-1} with the dust parameters in Table 3 inserted in Eqs. (1) and (10).

A clear linear relationship between $n_{250,\mathrm{d}}$ and σ_d is given which corroborates the usefulness of lidar for dust INP profiling after DeMott et al. (2010, 2015). The almost linear behavior of s_d with σ_d also suggests that surface-area-based INP parametzerization (Niemand et al., 2012; Steinke et al., 2015) for desert dust is possible with good accuracy. The relationship between $n_{250,\mathrm{d}}$ and σ_d values was already discussed by Mamouri and Ansmann (2015). However, as mentioned in Sect. 2.1, a wrong conversion factor was used in our foregoing article, the true one is $c_{250,\mathrm{d}} = 0.20\,\mathrm{Mm\,cm}^{-3}$.

4.3 Pure marine aerosol conditions

Barbados offers also the unique opportunity to analyze the relationship between the microphysical and optical properties for pure marine conditions. As mentioned, Barbados is located more than 4000 km west of Africa. No anthropogenic aerosol sources exist upwind Barbados over the tropical Atlantic (except ships). We selected 123 AERONET Barabados Ragged Point observations (level 2.0, 2007-2015) for our correlation study. To identify these pure marine conditions we used the criteria of AOT<0.07 at 500 nm and AE between 0.25–0.6. The AE value for pure marine conditions is clearly higher than for Saharan dust and smaller for cases with local pollution (mainly biomass burning). The marine AE values accumulate at 0.45-0.55. The conversion parameters for pristine marine conditions are given in Table 3.

As mentioned, because of the high relative humidity around 80% in the marine PBL, we use $n_{100,\mathrm{m}}$ as a proxy for $n_{50,\mathrm{m,dry}}$. Similarly $s_\mathrm{m}/4$ is assumed to represent $s_\mathrm{m,dry}$.

As for desert dust, the comparison with the CCN-σ correlation studies of Shinozuka et al. (2015) show good agreement. On Graciosa Island (Azores), for marine conditions (in summer, AE between 0.3 and 0.5), on average, $n_\mathrm{CCN} \approx 400 - 500\,\mathrm{cm}^{-3}$ was observed for a supersaturation of 0.3-0.5% and a mean dry extinction coefficient of 20 Mm^{-1}. For relative humidities of 80% the ambient extinction coefficients are roughly a factor of 3 larger than the dry extinction coefficients, and thus around 60 Mm^{-1} (Zieger et al., 2010; Zhang et al., 2014). By further assuming that the average $n_\mathrm{CCN} \approx 200 - 250\,\mathrm{cm}^{-3}$ when changing the supersaturation level from 0.3-0.5% to 0.2%, these transformed values are close to the ones obtained with our parameterization drawn

from the AERONET observations. By using the parameters in Table 3 and Eqs. (3) and (12), we get $n_{\mathrm{CCN}} \approx 200\,\mathrm{cm}^{-3}$ for an ambient $\sigma_{\mathrm{m}} = 50\ \mathrm{Mm}^{-1}$.

The good agreement between our parameterization and the CCNC-σ correlation study of Shinozuka et al. (2015) suggests that our way to handle the water uptake effect by using $n_{100,\mathrm{m}}$ as a proxy for $n_{50,\mathrm{m,dry}}$ is reasonable. Similarly, the good agreement with the results of Shinozuka et al. (2015), discussed in Sect. 4.2, indicates that the use of $n_{100,\mathrm{d}}$ (in the case of hydrophobic dust particles) to estimate dust $n_{\mathrm{CCN,d}}$ is justified, too.

4.4 Continental, marine, and desert aerosol conversion parameters and uncertainties

Figure 7 provides finally an overview of all 532 nm mean conversion parameters for the three aerosol types and different AERONET data sets. Clear differences in the conversion parameters for dust, marine, and continental (urban) aerosol conditions are visible. The error bars are related to the atmospheric variability (scatter in the correlations shown in Figs. 4-6). In Table 3, all conversion parameters (with corresponding SD) required to solve the equations in Sect. 3 are given for the three laser wavelengths.

Typical uncertainties in the basic particle optical properties, the derived particle number and surface area concentrations, and the CCN-relevant particle and INP number concentrations are provided in Table 4. They result from uncertainties in the lidar retrievals (uncertainties in the input parameters, statistical noise), and retrieval uncertainties as discussed in Sects. 2, 3, and 4. The uncertainties are similar for all three laser wavelengths.

The parameterizations and corresponding uncertainties given in Table 4 hold for relative humidities up to about 80% in the case of continental aerosols. The estimated n_{CCN} values are no longer trustworthy for higher relative humidities, i.e., for example in the subcloud layer (from 500 m below cloud base to cloud base), i.e., in the humid layer right below the base of a convective cloud system (Schmidt et al., 2014). It remains to be investigated to what extend our method can be used for relative humidities >80% and also for humidities <40%.

Further uncertainty sources, not considered in Table 4, are the unknown updraft velocities at cloud base so that n_{CCN} can easily be underestimated by a factor of 2-3 when the supersaturation is between 0.4–1% instead of 0.15% (as we assume). In the case of mineral dust the amount of soluble material on the dust particle surface sensitively influences the ability to act CCN so that n_{CCN} of aged dust particles coated with hygroscopic species may be a factor of 2-4 higher than predicted by our parameterization. As mentioned in Sect. 3.3, the derived $n_{\mathrm{CCN},ss=0.15\%}$ values can be interpreted as the minimum values of the possible solution space of $n_{\mathrm{CCN},ss}$ for ss from 0.1 to 1%.

Nevertheless, the consistency with the direct observations of CCNC and extinction coefficients by (Shinozuka et al., 2015) for marine, desert, and continental aerosol conditions corroborates that our lidar-based parameterizations are trustworthy. However, because the CCN retrievals based on the Leipzig and Limassol AERONET data sets for continental aerosols represent urban conditions, this parameterization may overestimate n_{CCN} in rural environments (aerosol background conditions) and probably also in the free troposphere (aged, long-range transported particles). It may be therefore advisable to use at least two sets of parameterizations for urban and rural sites and for the PBL (regional aerosol, high amount of freshly produced fine-mode particles) and the free troposphere (aged particles, partly originating from other continents) instead of just one generalized parameterization scheme. This aspect is further discussed in the next section.

5 Lidar estimates of $n_{\mathrm{CCN},ss}$ and n_{INP} profiles: case studies

In this section, we apply the developed methodology presented in Sect. 3 to two lidar observations. The first lidar measurement was performed recently during a strong dust outbreak crossing Cyprus in the spring of 2015. The second case was measured during an episode with continental aerosol pollution advected from the European continent to Cyprus in the summer of 2012.

5.1 Lidar profiling during a dust outbreak

During the BACCHUS field campaign in March-April 2015, described in Sect. 2.2, many dust outbreaks from the Middle East deserts and the Sahara were observed over Cyprus. We selected the case from 7 April to apply our methods to a dust-dominated aerosol scenario. The basic lidar observations of height profiles of particle backscatter, linear depolarization ratio, and derived σ_i profiles were already shown in Fig. 2. The σ_i profiles for 532 nm wavelength are the input parameters for the retrieval of the particle number concentrations $n_{50,\mathrm{dry}}$, $n_{100,\mathrm{dry}}$, and $n_{250,\mathrm{dry}}$, and of the particle surface area concentration s_{dry} shown in Fig. 8. Equations (1)–(9) and the conversion parameters in Table 3 are used to obtain the presented profiles. For desert dust we used the SAMUM/SALTRACE conversion parameters, for continental pollution the Leipzig data, and for marine aerosols the Barbados (2007–2015) conversion parameters. The error bars indicate typical uncertainties (as summarized in Table 4). For $n_{50,\mathrm{dry}}$ and $n_{100,\mathrm{dry}}$ we simply assume an overall uncertainty factor of 2 in Fig. 8 (and in the following figures also for n_{CCN}). For $n_{250,\mathrm{dry}}$ and s_{dry} the error bars show relative uncertainties of 30% (dust) to 50% (continental aerosol).

As can be seen in Fig. 8, the fine-mode-dominated continental aerosol fraction contains more CCN-relevant small particles ($n_{50,\mathrm{dry}}$ vs $n_{100,\mathrm{dry}}$) than the desert aerosol, although the ambient extinction coefficients σ_c are smaller than the dust-related σ_d values. Vice versa, the coarse-mode-dominated dust aerosol controls the overall large-particle number concentrations $n_{250,\mathrm{dry}}$ and surface area concentration s_{dry}.

Figure 9 shows the retrieval products in terms of n_{CCN} and n_{INP}. In addition, the GDAS temperature and relative humidity (RH) profiles are given. Different n_{CCN} retrievals are presented. The profiles for GE(c) (thick green profile in Figure 9) and for CY(c) (thin light green profile) are calculated with Eq. (11) and the conversion parameters for Leipzig (GE for Germany) and Limassol (CY for Cyprus) for continental aerosol (c) in Table 3, respectively. For comparison, also results obtained with the generalized parameterization scheme of Shinozuka et al. (2015) for a supersaturation level of 0.2% and the AE class of 1.5-1.7 are plotted (SHI(c), thin green profile in Figure 9). In our notation (according to Eq. 11), the SHI(c) parameters in Figure 9 are $c_{\mathrm{CCN}} = 30\ \mathrm{cm}^{-3}$ (for $\sigma = 1\ \mathrm{Mm}^{-1}$) and $x_{\mathrm{CCN}} = 0.75$, and represent rural-like rather than urban aerosol conditions. Similarly, the correlation study of Sakai et al. (2013) based on vertical profiles of ambient particle backscatter coefficients measured with lidar over southern Japan and airborne in situ CCN observations, yield $c_{\mathrm{CCN}} = 30\ \mathrm{cm}^{-3}$ (for $\sigma = 1\ \mathrm{Mm}^{-1}$), but $x_{\mathrm{CCN}} = 0.5$. These observations also indicate aerosol background conditions (AE values mostly from 0.3-1.0). As mentioned above, we used an extinction-to-backscatter ratio of 50 sr to transfer the backscatter into extinction coefficients at 532 nm laser wavelength.

The desert-dust-related n_{CCN} profile (thick red curve in Fig. 9) is calculated with Eq. (10) and the conversion parameters in Table 3, derived from the Cabo-Verde and Barbados AERONET observations of pure dust (denoted as CV-BB(d)). Again for comparison, the thin orange profile (SHI(d)) shows the n_{CCN} profile obtained with the generalized aerosol parameterization of Shinozuka et al. (2015) for the supersaturation level of 0.2% and AE from 0.3-0.5. The SHI(d) conversion parameters are in this case $c_{\mathrm{CCN}} = 13\ \mathrm{cm}^{-3}$ (for $\sigma_\mathrm{d} = 1\ \mathrm{Mm}^{-1}$) and $x_{\mathrm{CCN}} = 0.75$. It is interesting to note that the Limassol dust conversion parameters in Table 3 ($c_{100,\mathrm{d}} = 11.8\ \mathrm{cm}^{-3}$ for $\sigma_\mathrm{d} = 1\ \mathrm{Mm}^{-1}$, $x_\mathrm{d} = 0.76$) and the Leipzig dust conversion parameters ($c_{100,\mathrm{d}} = 13.9\ \mathrm{cm}^{-3}$ for $\sigma_\mathrm{d} = 1\ \mathrm{Mm}^{-1}$, $x_\mathrm{d} = 0.73$) are similar to the SHI(d) conversion parameters. All three parameterizations obviously represent slightly polluted desert dust conditions. For pure desert dust scenarios (CV-BB(d), thick red profile in Fig. 9, based on the Cabo-Verde and Barbados AERONET observations) the respective n_{CCN} values are lower by almost a factor of 2.

The different profiles for continental aerosols (GE(c), CY(c), and SHI(c)) provide an impression of the uncertainty in the n_{CCN} retrieval for this aerosol type. Similarly, the orange and red curves may indicate the overall uncertainty in the retrieval of n_{CCN} for desert dust.

The relative humidity profile indicates, that RH is <80% for the range from 1-6 km height. For this region, our parameterization (for RH around 60%±20%) is valid. Care has to be taken in the interpretation of the continental n_{CCN} values in the PBL (RH>80%) and in the upper troposphere (above 6 km height, RH>80%).

In the central panel of Fig. 9, the retrieved INP profiles are shown, obtained with the different parameterizations discussed in Sect. 3.4. Mamouri and Ansmann (2015) already discussed the retrieval of n_{INP} from $n_{250,\mathrm{d}}$ by using the D10 method (DeMott et al., 2010) and the D15 approach (DeMott et al., 2015). Figure 9 also contains the n_{INP} profiles when the desert particle surface-area concentration s_d is used as input in the N12 approach (Niemand et al., 2012) and S15 parameterization (Steinke et al., 2015). Because air temperatures are all above $0\,^\circ\mathrm{C}$ at heights below $3.6\,\mathrm{km}$ as the horizontal temperature lines in Fig. 9 (right panel) indicate, n_{INP} values are only given for the upper part of the desert dust plume. According to Table 4, the uncertainty in the INP retrieval is within a factor of 3-10.

It is not the aim of the paper to discuss in detail the reasons for the differences between the different immersion freezing parameterizations of DeMott et al. (2015) and Niemand et al. (2012), which partly exceed one order of magnitude. The higher n_{INP} values obtained with the procedure developed by Niemand et al. (2012) compared to the one presented by DeMott et al. (2015) may result from the fact that s covers all particles even particles with radius $< 250\,\mathrm{nm}$. The combination of the parameterizations of Niemand et al. (2012) (dust aerosol, immersion freezing) and Steinke et al. (2015) (dust, deposition freezing) provides the opportunity to deliver n_{INP} profiles from about -10 to $-50\,^\circ\mathrm{C}$ and thus up to cirrus level. The parametrization scheme of Steinke et al. (2015) need to be tested for natural desert dust. As mentioned in Sect 3.4.2, it is based on laboratory studies with Arizona test dust.

At the end of this subsection, it is noteworthy to mention that similar profiles as shown in Figs. 8 and 9 can be obtained with a polarization lidar operated at the laser wavelength of $355\,\mathrm{nm}$. The respective conversion parameters are given in Table 3. This means that ESA's EarthCARE lidar (satellite-borne $355\,\mathrm{nm}$ polarization/HSR lidar) (Illingworth et al., 2015a) can also provide these CCN and INP number concentration profiles, however on a global scale.

5.2 Lidar profiling during an episode with European continental pollution

In contrast to the BACCHUS dust case in Fig. 2, the backscatter and depolarization profiles in Fig. 10 show a case with strong advection of aerosol from the European continental. The measurement was taken at Limassol on 16 August

2012. The AOT at 532 nm was about 0.2 and AE close to 1.8. Aerosols up to 3.5 km height were detected and the air masses came from northern to northwestern directions, from Europe and Turkey according to backward trajectory analysis. We used lidar ratios of 50–60 sr for continental pollution and 45 sr for mineral dust in the backscatter-to-extinction conversion to obtain the σ_i profiles from the backscatter coefficients. We again assume a small contribution of marine particles in the boundary layer over the coastal city of Limassol. The almost height-independent particle linear depolarization ratio indicates an aged, well-mixed pollution plume. The values of the depolarization ratio are 5-8 %. Such values indicate the presence of a small amount of soil and road dust, or even traces of desert dust.

Figure 11 shows the derived profiles of the CCN-relevant particle number concentration n_{CCN} and of the INP-relevant $n_{250,\mathrm{dry}}$ values. The respective n_{INP} values are at all zero for this case with ambient temperatures $>0\,^{\circ}\mathrm{C}$ up to 5 km height, as shown in the right panel.

Most interesting for such a pollution case in the lower troposphere are the n_{CCN} profiles. We show again the profiles for different parameterization. The Limassol conversion parameters (CY(c)), the Leipzig parameters (GE(c)), and the parameterization after Shinozuka et al. (2015) for the supersaturation level of 0.2% and AE around 1.6 (SHI(c)) are applied. The contributions of the dust and marine aerosol components (20-40 cm^{-3}) to n_{CCN} are almost negligible in this case.

The overall uncertainty in the retrieval of a factor of 3 is again well covered by the three different parameterizations. Because the relative humidity is mostly between 40-60% an RH-related error can be regarded to be small. As can be seen, even at moderate pollution levels with σ_{c} of 30-60 Mm^{-1}, the n_{CCN} values can be of the order of 1000-2000 cm^{-3} at urban sites. By using the parameterization of Shinozuka et al. (2015) (SHI(c) profile), which is more appropriate for rural aerosol conditions, we obtain $n_{\mathrm{CCN}} \approx 300-500\ \mathrm{cm}^{-3}$.

6 Conclusions

For the first time, a comprehensive study on the potential of polarization lidar to provide vertical profiles of CCN-relevant particle and INP number concentrations has been presented. Of key importance is the separation of the basic aerosol types (desert, continental, marine) by means of the polarization lidar technique. Based on an in-depth correlation study applied to long-term and field campaign AERONET observations, it is has been demonstrated that a solid way exists from the particle extinction coefficients, as measurable with lidar, to the basic aerosol parameters from which the n_{CCN} and n_{INP} profiles can be estimated.

We showed that height profiles of CCN-relevant number concentrations of aerosol particles with dry radius $>50\,\mathrm{nm}$ (marine and continental particles) and $>100\,\mathrm{nm}$ (desert dust), and of the INP-relevant number concentration of particles with dry radius $>250\,\mathrm{nm}$, as well as profiles of the aerosol particle surface area concentration can be retrieved from lidar-derived aerosol extinction coefficients with relative uncertainties of a factor of around 2 (CCN reservoir) and about 25–50 % (INP reservoir). The overall uncertainties in the n_{CCN} estimation of a factor 3 and in the n_{INP} estimation of a factor 3-10 result, to a large extent, from the unknown aerosol types and properties (origin of the aerosol components, chemical composition of the aerosol, aging and coating effects).

The full methodology was applied to two contrasting cases: a heavy desert dust outbreak crossing Cyprus with mineral dust up to 8 km height in the spring of 2015 and a case with aged anthropogenic haze from the European continent. These case studies clearly demonstrated the attractiveness of lidar to provide simultaneously height profiles of n_{CCN} and n_{INP} estimates up to the mixed-phase and cirrus cloud level.

There is room for improvements. Our study may be regarded as a starting point for a deeper discussion on the role of lidar (organized in ground-based networks and operated in space) to provide height profiles of cloud-relevant aerosol parameters and to support in this way atmospheric research regarding the aerosol impact on cloud evolution and precipitation formation processes. It is an open question how to handle the water-uptake effect by the particles in the retrieval of the required dry-particle microphysical properties. Should one also move from lidar-derived ambient particle extinction coefficients to dry-particle extinction coefficients as in the study of (Shinozuka et al., 2015)? Can we significantly improve the accurracy in the n_{CCN} and n_{INP} retrievals by combining the polarization lidar technique with the Raman lidar technique for water vapor and temperature profiling so that actual height profiles for relative humidity (Mattis et al., 2002) are available for the necessary water-uptake corrections? Do we need at least two CCN parameterization schemes to cover contrasting environments (rural versus urban sites, PBL versus free tropospheric height regions)? In this context we may follow the way of Sakai et al. (2013) to use the AE profile (measured in the case of a multiwavelength lidar) as a guide in the selection of the most appropriate CCN parameterization scheme? Regarding n_{INP} profiling, the question arises, in which way we may better consider the different INP efficacy of different aerosol types in the INP parameterizations, especially in cases with good knowledge on the amount of biological particles, biomass burning smoke, or urban haze in observed complex aerosol mixtures as a function of site, season of the year, and height range in close combination with backward trajectory analysis or more complex aerosol transport modeling? All these questions need to be answered in followup studies.

Our future plans comprise extended comparisons of the lidar observations of n_{CCN} and n_{INP} profiles with respec-

tive surface and airborne in-situ observations of these quantities. The efforts should also include comparisons of the basic aerosol parameters such as $n_{50,\mathrm{dry}}$, $n_{100,\mathrm{dry}}$, and $n_{250,\mathrm{dry}}$, and the surface area concentration s_{dry}. Several measurement campaigns and long-term monitoring aerosol data sets will be used in these quality assurance activities. We will, e.g., compare the lidar retrieval products with aircraft measurements of desert-dust and marine-aerosol-related CCNC profiles, collected during the SALTRACE–1 campaign (Barbados, 2013) and with ground-based in-situ n_{INP} observations during the BACCHUS campaign (Cyprus, 2015).

Furthermore, it is time for well-designed INP campaigns with aircraft measurements around laser beams. Airborne in situ observations (including aboard unmanned aerial vehicles, UAVs) in a desert environment, at pure marine conditions, and at mixed aerosol conditions would be desirable. The aerosol components (origin, chemical composition), the particle size distributions, and INP number concentrations need to be measured in the vicinity or around the laser beams of a polarization lidar. Such field campaigns would provide ideal conditions for in-depth characterization of the potential of lidar-based INP parameterization efforts. This would also provide the unique opportunity to identify the gaps in our knowledge regarding heterogeneous ice formation when combined with cloud observations. The lidar monitors the evolution of cloud layers (altocumulus and cirrus layers) embedded in the aerosol layers from cloud base to cloud top, whereas aircraft can probe the aerosol and cloud layers, height level by height level, in terms of ice crystal and INP number concentrations.

Acknowledgements. We thank Ronny Engelmann and Johannes Bühl from TROPOS for performing the BACCHUS lidar measurements at Nicosia. We are grateful to Margit Pattantyús-Ábrahám, Meteorological Observatory Hohenpeissenberg, for the 20-year radiosonde data analysis, Heike Wex (TROPOS) for fruitful discussion on CCNC and INP characteristisc for a variety of aerosol types, Patric Seifert (TROPOS) for providing a critical analysis of RH profile effects on the extinction coefficient, Annett Skupin (TROPOS) for providing measured relationships between aerosol microphysical properties and long-term ambient extinction data at the TROPOS site, and Maximilian Dollner (Meteorological Institute, Munich University) for providing CCNC profile data measured during the SALTRACE 2013 campaign. The authors also thank the CUT Remote Sensing Laboratory (especially Argyro Nisantzi) for careful lidar and photometer observations at Limassol during many years. Special thanks to Joe Prospero and his team (University of Miami) for taking care of all the good Ragged Point AERONET observations. We are also grateful to the National Observatory of Athens (NOA) for providing the Polly lidar for the six-week BACCHUS field campaign in 2015. The NOA Polly lidar was supported by the European Union Seventh Framework Programme (FP7-REGPOT-2012–2013-1), in the framework of the project BEYOND, under grant agreement no. 316210 (BEYOND – Building Capacity for a Centre of Excellence for EO-based monitoring of Natural Disasters). We thank the Cyprus Institute for support and the very pleasant field campaign conditions at Nicosia. AERONET has to be mentioned here for high-quality sun/sky photometer measurements in Cyprus, Germany, Morocco, Cape Verde, and Barbados and respective the high quality data analysis. The authors acknowledge AERONET-Europe for providing calibration service. AERONET-Europe is part of ACTRIS-2 project that received funding from the European Union (H2020-INFRAIA-2014-2015) under Grant Agreement No 654109. This work was co-funded by the European Regional Development Fund and the Republic of Cyprus through the Research Promotion Foundation (PENEK/0311/05). We acknowledge funding from the EU FP7-ENV-2013 programme "impact of Biogenic vs. Anthropogenic emissions on Clouds and Climate: towards a Holistic UnderStanding" (BACCHUS), project number 603445.

References

Andreae, M. O.: Correlation between cloud condensation nuclei concentration and aerosol optical thickness in remote and polluted regions, Atmos. Chem. Phys., 9, 543–556, doi:10.5194/acp-9-543-2009, 2009.

Ansmann, A., Bösenberg, J., Chaikovsky, A., Comerón, A., Eckhardt, S., Eixmann, R., Freudenthaler, V., Ginoux, P., Komguem, L., Linné, H., López Márquez, M. A., Matthias, V., Mattis, I., Mitev, V., Müller, D., Music, S., Nickovic, S., Pelon, J., Sauvage, L., Sobolewsky, P., Srivastava, M. K., Stohl, A., Torres, O., Vaughan, G., Wandinger, U., and Wiegner, M.: Long-range transport of Saharan dust to northern Europe: the 11–16 October 2001 outbreak observed with EARLINET, J. Geophys. Res., 108, 4783, doi:10.1029/2003JD003757, 2003.

Ansmann, A., Wandinger, U., Le Rille, O., Lajas, D., and Straume, A. G.: Particle backscatter and extinction profiling with the spaceborne high-spectral-resolution Doppler lidar ALADIN: methodology and simulations, Appl. Optics, 46, 6606–6626, 2007.

Ansmann, A., Tesche, M., Seifert, P., Althausen, D., Engelmann, R., Fruntke, J., Wandinger, U., Mattis, I., and Müller, D.: Evolution of the ice phase in tropical altocumulus: SAMUM lidar observations over Cape Verde, J. Geophys. Res., 114, D17208, doi:10.1029/2008JD011659, 2009.

Ansmann, A., Petzold, A., Kandler, K., Tegen, I., Wendisch, M., Müller, D., Weinzierl, B., Müller, T., and Heintzenberg, J.: Saharan mineral dust experiments SAMUM-1 and SAMUM-2: what have we learned?, Tellus B, 63, 403–429, doi:10.1111/j.1600-0889.2011.00555.x, 2011a.

Ansmann, A., Tesche, M., Seifert, P., Groß, S., Freudenthaler, V., Apituley, A., Wilson, K. M., Serikov, I., Linné, H., Heinold, B., Hiebsch, A., Schnell, F., Schmidt, J., Mattis, I., Wandinger, U., and Wiegner, M.: Ash and fine-mode particle mass profiles from EARLINET-AERONET observations over central Europe after the eruptions of the Eyjafjallajökull volcano in 2010, J. Geophys. Res., 116, D00U02, doi:10.1029/2010JD015567, 2011b.

Ansmann, A., Seifert, P., Tesche, M., and Wandinger, U.: Profiling of fine and coarse particle mass: case studies of Saharan dust and Eyjafjallajökull/Grimsvötn volcanic plumes, Atmos. Chem. Phys., 12, 9399–9415, doi:10.5194/acp-12-9399-2012, 2012.

Augustin, S., Wex, H., Niedermeier, D., Pummer, B., Grothe, H., Hartmann, S., Tomsche, L., Clauss, T., Voigtländer, J., Ignatius, K., and Stratmann, F.: Immersion freezing of birch

pollen washing water, Atmos. Chem. Phys., 13, 10989–11003, doi:10.5194/acp-13-10989-2013, 2013.

Augustin-Bauditz, S., Wex, H., Kanter, S., Ebert, M., Stolz, F., Prager, A., Niedermeier, D., and Stratmann, F.: The immersion mode ice nucleation behavior of mineral dusts: a comparison of different pure and surface modified dusts, Geophys. Res. Lett., 41, 7375–7382, doi:10.1002/2014GL061317, 2014.

Baars, H., Ansmann, A., Althausen, D., Engelmann, R., Heese, B., Müller, D., Artaxo, P., Paixao, M., Pauliquevis, T., and Souza, R.: Aerosol profiling with lidar in the Amazon Basin during the wet and dry season, J. Geophys. Res., 117, D21201, doi:10.1029/2012JD018338, 2012.

Baars, H., Kanitz, T., Engelmann, R., Althausen, D., Heese, B., Komppula, M., Preißler, J., Tesche, M., Ansmann, A., Wandinger, U., Lim, J.-H., Ahn, J. Y., Stachlewska, I. S., Amiridis, V., Marinou, E., Seifert, P., Hofer, J., Skupin, A., Schneider, F., Bohlmann, S., Foth, A., Bley, S., Pfüller, A., Giannakaki, E., Lihavainen, H., Viisanen, Y., Hooda, R. K., Pereira, S., Bortoli, D., Wagner, F., Mattis, I., Janicka, L., Markowicz, K. M., Achtert, P., Artaxo, P., Pauliquevis, T., Souza, R. A. F., Sharma, V. P., van Zyl, P. G., Beukes, J. P., Sun, J. Y., Rohwer, E. G., Deng, R., Mamouri, R. E., and Zamorano, F.: Polly^{NET}: a global network of automated Raman-polarization lidars for continuous aerosol profiling, Atmos. Chem. Phys. Discuss., 15, 27943–28004, doi:10.5194/acpd-15-27943-2015, 2015.

Barnaba, F. and Gobbi, G. P.: Lidar estimation of tropospheric aerosol extinction, surface area and volume: maritime and desert-dust cases, J. Geophys. Res., 106, 3005–3018, doi:10.1029/2000JD900492, 2001.

Barnaba, F. and Gobbi, G. P.: Correction to "Lidar estimation of tropospheric aerosol extinction, surface area and volume: maritime and desert-dust cases" by F. Barnaba and G. P. Gobbi, J. Geophys. Res., 107, 4180, doi:10.1029/2002JD002340, 2002.

Bangert , M., Nenes, A., Vogel, B., Vogel, H., Barahona, D., Karydis, V. A., Kumar, P., Kottmeier, C., and Blahak, U.: Saharan dust event impacts on cloud formation and radiation over Western Europe, Atmos. Chem. Phys., 12, 4045-4063, doi:10.5194/acp-12-045-2012, 2012.

Bates, T. S., Quinn, P. K., Covert, D. S., Coffman, D. J., Johnson, J. E., and Wiedensohler, A.: Aerosol physical properties and processes in the lower marine boundary layer: a comparison of shipboard sub-micron data from ACE-1 and ACE-2, Tellus B, 52, 258–272, doi:10.1034/j.1600-0889.2000.00021.x, 2000.

Beddows, D. C. S., Dall'Osto, M., Harrison, R. M., Kulmala, M., Asmi, A., Wiedensohler, A., Laj, P., Fjaeraa, A. M., Sellegri, K., Birmili, W., Bukowiecki, N., Weingartner, E., Baltensperger, U., Zdimal, V., Zikova, N., Putaud, J.-P., Marinoni, A., Tunved, P., Hansson, H.-C., Fiebig, M., Kivekäs, N., Swietlicki, E., Lihavainen, H., Asmi, E., Ulevicius, V., Aalto, P. P., Mihalopoulos, N., Kalivitis, N., Kalapov, I., Kiss, G., de Leeuw, G., Henzing, B., O'Dowd, C., Jennings, S. G., Flentje, H., Meinhardt, F., Ries, L., Denier van der Gon, H. A. C., and Visschedijk, A. J. H.: Variations in tropospheric submicron particle size distributions across the European continent 2008–2009, Atmos. Chem. Phys., 14, 4327–4348, doi:10.5194/acp-14-4327-2014, 2014.

Bühl, J., Ansmann, A., Seifert, P., Baars, H., and Engelmann, R.: Toward a quantitative characterization of heterogeneous ice formation with lidar/radar: comparison of CALIPSO/CloudSat with ground-based observations, Geophys. Res. Lett., 40, 4404–4408, doi:10.1002/grl.50792, 2013.

Comstock, J. M., Lin, R.-F., Starr, D. O'C., and Yang, P.: Understanding ice supersaturation, particle growth, and number concentration in cirrus clouds, J. Geophys. Res., 113, D23211, doi:10.1029/2008JD010332, 2008.

de Boer, G., Morrison, H., Shupe, M. D., and Hildner, R.: Evidence of liquid dependent ice nucleation in high-latitude stratiform clouds from surface remote sensors, Geophys. Res. Lett., 38, L01803, doi:10.1029/2010GL046016, 2011.

DeMott, P. J., Prenni, A. J., Liu, X., Kreidenweis, S. M., Petters, M. D., Twohy, C. H., Richardson, M. S., Eidhammer, T., and Rogers, D. C.: Predicting global atmospheric ice nuclei distributions and their impacts on climate, P. Natl. Acad. Sci. USA, 107, 11217–11222, doi:10.1073/pnas.0910818107, 2010.

DeMott, P. J., Prenni, A. J., McMeeking, G. R., Sullivan, R. C., Petters, M. D., Tobo, Y., Niemand, M., Möhler, O., Snider, J. R., Wang, Z., and Kreidenweis, S. M.: Integrating laboratory and field data to quantify the immersion freezing ice nucleation activity of mineral dust particles, Atmos. Chem. Phys., 15, 393–409, doi:10.5194/acp-15-393-2015, 2015.

DeMott, P. J., Hill, T. C. J., McCluskey, C. S., Prather, K. A., Collins, D. B., Sullivan, R. C., Ruppel, M. J., Mason, R. H., Irish, V. E., Lee, T., Hwang, C. Y., Rhee, T. S., Snider, J. R., McMeeking, G. R., Dhaniyala, S., Lewis, E. R., Wentzell, J. J. B., Abbatt, J., Lee, C., Sultana, C. M., Ault, A. P., Axson, J. L., Martinez, M. D., Venero, I., Santos-Figueroa, G., Dale Stokes, M. Deane, G. B., Mayol-Bracero, O. L., Grassian, V. H., Bertram, T. H., Bertram, A. K., Moffett, B. F., and Franc, G. D.: Sea spray aerosol as a unique source of ice nucleating particles, P. Natl. Acad. Sci. USA, 113, pages...., doi:10.1073/pnas.1514034112, 2016.

Deng, Z. Z., Zhao, C. S., Ma, N., Liu, P. F., Ran, L., Xu, W. Y., Chen, J., Liang, Z., Liang, S., Huang, M. Y., Ma, X. C., Zhang, Q., Quan, J. N., Yan, P., Henning, S., Mildenberger, K., Sommerhage, E., Schäfer, M., Stratmann, F., and Wiedensohler, A.: Size-resolved and bulk activation properties of aerosols in the North China Plain, Atmos. Chem. Phys., 11, 3835–3846, doi:10.5194/acp-11-3835-2011, 2011.

Ditas, F., Shaw, R. A., Siebert, H., Simmel, M., Wehner, B., and Wiedensohler, A.: Aerosols-cloud microphysics-thermodynamics-turbulence: evaluating supersaturation in a marine stratocumulus cloud, Atmos. Chem. Phys., 12, 2459–2468, doi:10.5194/acp-12-2459-2012, 2012.

Dubovik, O. and King, M.: A flexible inversion algorithm for retrieval of aerosol optical properties from sun and sky radiance measurements, J. Geophys. Res., 105, 20673–20696, doi:10.1029/2000JD900282, 2000.

Dubovik, O., Smirnov, A., Holben, B. N., King, M. D., Kaufman, Y. J., Eck, T. F., and Slutsker, I.: Accuracy assessments of aerosol optical properties retrieved from Aerosol Robotic Network (AERONET) Sun and sky radiance measurements, J. Geophys. Res., 105(D8), 9791-9806, doi:10.1029/2000JD900040, 2000.

Dubovik, O., Sinyuk, A., Lapyonok, T., Holben, B. N., Mishchenko, M., Yang, P., Eck, T. F., Voltne, H., Munoz, O., Veihelmann, B., Van der Zande, W. J., Leon, J.-F., Sorokin, M., and Slutsker, I.: Application of spheroid models to account for aerosol particle nonsphericity in remote sensing of desert dust, J.

Geophys. Res., 111, D11208, doi:10.1029/2005JD006619, 2006.

Ebert, M., Worringen, A., Benker, N., Mertes, S., Weingartner, E., and Weinbruch, S.: Chemical composition and mixing-state of ice residuals sampled within mixed phase clouds, Atmos. Chem. Phys., 11, 2805–2816, doi:10.5194/acp-11-2805-2011, 2011.

Engelmann, R., Kanitz, T., Baars, H., Heese, B., Althausen, D., Skupin, A., Wandinger, U., Komppula, M., Stachlewska, I. S., Amiridis, V., Marinou, E., Mattis, I., Linné, H., and Ansmann, A.: EARLINET Raman Lidar Polly^{XT}: the neXT generation, Atmos. Meas. Tech. Discuss., 8, 7737–7780, doi:10.5194/amtd-8-7737-2015, 2015.

Freudenthaler, V., Esselborn, M., Wiegner, M., Heese, B., Tesche, M., Ansmann, A., Müller, D., Althausen, D., Wirth, M., Fix, A., Ehret, G., Knippertz, P., Toledano, C., Gasteiger, J., Garhammer, M., and Seefeldner, M.: Depolarization ratio profiling at several wavelengths in pure Saharan dust during SAMUM 2006, Tellus B, 61, 165–179, doi:10.1111/j.1600-0889.2008.00396.x, 2009.

Ghan, S. J. and Collins, D. R.: Use of In situ data to test a raman lidar-based cloud condensation nuclei remote sensing method, J. Atmos. Ocean. Tech., 21, 387–394, doi:10.1175/1520-0426(2004)021<0387:UOISDT>2.0.CO;2, 2004.

Ghan, S. J., Rissman, T. A., Elleman, R., Ferrare, R. A., Turner, D., Flynn, C., Wang, J., Ogren, J., Hudson, J., Jonsson, H. H., Van-Reken, T., Flagan, R. C., and Seinfeld, J. H.: Use of in situ cloud condensation nuclei, extinction, and aerosol size distribution measurements to test a method for retrieving cloud condensation nuclei profiles from surface measurements, J. Geophys. Res., 111, D05S10, doi:10.1029/2004JD005752, 2006.

Groß, S., Tesche, M., Freudenthaler, V., Toledano, C., Wiegner, M., Ansmann, A., Althausen, D., and Seefeldner, M.: Characterization of Saharan dust, marine aerosols and mixtures of biomass-burning aerosols and dust by means of multi-wavelength depolarization and Raman lidar measurements during SAMUM 2, Tellus B, 63, 706–724, doi:10.1111/j.1600-0889.2011.00556.x, 2011.

Groß, S., Esselborn, M., Weinzierl, B., Wirth, M., Fix, A., and Petzold, A.: Aerosol classification by airborne high spectral resolution lidar observations, Atmos. Chem. Phys., 13, 2487–2505, doi:10.5194/acp-13-2487-2013, 2013.

Groß, S., Freudenthaler, V., Schepanski, K., Toledano, C., Schäfler, A., Ansmann, A., and Weinzierl, B.: Optical properties of long-range transported Saharan dust over Barbados as measured by dual-wavelength depolarization Raman lidar measurements, Atmos. Chem. Phys., 15, 11067-11080, doi:10.5194/acp-15-11067-2015, 2015.

Haarig, M., Althausen, D., Ansmann, A., Klepel, A., Baars, H., Engelmann, R., Groß, S., and Freudenthaler, V.: Measurement of the linear depolarization ratio of aged dust at three wavelengths (355, 532 and 1064 nm) simultaneously over Barbados, in: Proceedings of the 27th Interntaional Laser Radar Conference, New York City, 5–10 July 2015, S8b.04, 2015.

Hartmann, S., Augustin, S., Clauss, T., Wex, H., Šantl-Temkiv, T., Voigtländer, J., Niedermeier, D., and Stratmann, F.: Immersion freezing of ice nucleation active protein complexes, Atmos. Chem. Phys., 13, 5751–5766, doi:10.5194/acp-13-5751-2013, 2013.

Henning, S., Dieckmann, K., Ignatius, K., Schäfer, M., Zedler, P., Harris, E., Sinha, B., van Pinxteren, D., Mertes, S., Birmili, W., Merkel, M., Wu, Z., Wiedensohler, A., Wex, H., Herrmann, H., and Stratmann, F.: Influence of cloud processing on CCN activation behaviour in the Thuringian Forest, Germany during HCCT-2010, Atmos. Chem. Phys., 14, 7859–7868, doi:10.5194/acp-14-7859-2014, 2014.

Hiranuma, N., Kohn, M., Pekour, M. S., Nelson, D. A., Shilling, J. E., and Cziczo, D. J.: Droplet activation, separation, and compositional analysis: laboratory studies and atmospheric measurements, Atmos. Meas. Tech., 4, 2333–2343, doi:10.5194/amt-4-2333-2011, 2011.

Holben, B. N., Eck, T. F., Slutsker, I., Tanré, D., Buis, J. P., Setzer, A., Vermote, E., Reagan, J. A., Kaufman, Y. J., Nakajima, T., Lavenu, F., Jankowiak, I., and Smirnov, A.: AERONET – a federated instrument network and data archive for aerosol characterization, Remote Sens. Environ., 66, 1–16, 1998.

Illingworth, A. J., Hogan, R. J., O'Connor, E. J., Bouniol, D., Delanoe, J., Pelon, J., Protat, A., Brooks, M. E., Gaussiat, N., Wilson, D. R., Donovan, D. P., Klein Baltink, H., van Zadelhoff, G.-J., Eastment, J. D., Goddard, J. W. F., Wrench, C. L., Haeffelin, M., Krasnov, O. A., Russchenberg, H. W. J., Piriou, J.-M., Vinit, F., Seifert, A., Tompkins, A. M., and Willen, J., CLOUDNET: continuos evaluation of cloud profiles in seven operational models using ground-based observations, B. Am. Meteorol. Soc., 88, 883–898, 2007.

Illingworth, A. J., Barker, H. W., Beljaars, A., Ceccaldi, M., Chepfer, H., Clerbaux, N., Cole, J., Delanoe, J., Domenech, C., Donovan, D. P., Fukuda, S., Hirakata, M., Hogan, R. J., Huenerbein, H., Kollias, P., Kubota, T., Nakajima, T., Nakajima, T. Y., Nishizawa, T., Ohno, Y., Okamoto, H., Oki, R., Sato, K., Satoh, M., Shephard, M., Velázquez-Blázquez, A., Wandinger, U., Wehr, T., and Zadelhoff, G.-J.: THE EARTHCARE SATELLITE: the next step forward in global measurements of clouds, aerosols, precipitation and radiation, B. Am. Meteorol. Soc., 96, 1311–1332, doi:10.1175/BAMS-D-12-00227.1, 2015a.

Illingworth, A. J., Cimini, D., Gaffard, C., Haeffelin, M., Lehmann, V., Löhnert, U., O'Connor, E. J., and Ruffieux, D.: Exploiting Existing Ground-Based Remote Sensing Networks to Improve High-Resolution Weather Forecasts. B. Am. Meteorol. Soc., 96, 2107-2125, doi:10.1175/BAMS-D-13-00283.1, 2015b.

IPCC 2013: Climate Change 2013: The Physical Science Basis. Contribution of Working Group I to the Fifth Assessment Report of the Intergovernmental Panel on Climate Change, edited by: Stocker, T. F., Qin, D., Plattner, G.-K., Tignor, M., Allen, S. K., Boschung, J., Nauels, A., Xia, Y., Bex, V., and Midgley, P. M., Cambridge University Press, Cambridge, UK and New York, NY, USA, 1535 pp., available at: http://www.climatechange2013.org/images/report/WG1AR5_ALL_FINAL.pdf (last access: 29 January 2014), 2013.

Jefferson, A.: Empirical estimates of CCN from aerosol optical properties at four remote sites, Atmos. Chem. Phys., 10, 6855–6861, doi:10.5194/acp-10-6855-2010, 2010.

Ji, Q. and Shaw, G. E.: On supersaturation spectrum and size distributions of cloud condensation nuclei, Geophys. Res. Lett., 25, 1903–1906, doi:10.1029/98GL01404, 1998.

Kamphus, M., Ettner-Mahl, M., Klimach, T., Drewnick, F., Keller, L., Cziczo, D. J., Mertes, S., Borrmann, S., and Curtius, J.: Chemical composition of ambient aerosol, ice residues

and cloud droplet residues in mixed-phase clouds: single particle analysis during the Cloud and Aerosol Characterization Experiment (CLACE 6), Atmos. Chem. Phys., 10, 8077–8095, doi:10.5194/acp-10-8077-2010, 2010.

Kanitz, T., Seifert, P., Ansmann, A., Engelmann, R., Althausen, D., Casiccia, C., and Rohwer, E. G.: Contrasting the impact of aerosols at northern and southern midlatitudes on heterogeneous ice formation, Geophys. Res. Lett., 38, L17802, doi:10.1029/2011GL048532, 2011.

Kanitz, T., Ansmann, A., Engelmann, R., and Althausen, D.: North-south cross sections of the vertical aerosol distribution over the Atlantic Ocean from multiwavelength Raman/polarization lidar during Polarstern cruises, J. Geophys. Res. Atmos., 118, 2643-2655, doi:10.1002/jgrd.50273, 2013.

Kanitz, T., Engelmann, R., Heinold, B., Baars, H., Skupin, A., and Ansmann, A.: Tracking the Saharan Air Layer with shipborne lidar across the tropical Atlantic, Geophys. Res. Lett., 41, 1044–1050, doi:10.1002/2013GL058780, 2014.

Karydis, V. A., Kumar, P., Barahona, D., Sokolik, I. N., and Nenes, A.: On the effect of dust particles on global cloud condensation nuclei and cloud droplet number, J. Geophys. Res., 116, D23204, doi:10.1029/2011JD016283, 2011.

Koehler, K. A., Kreidenweis, S. M., DeMott, P. J., Petters, M-D., Prenni, A. J., and Carrico, C. M.: Hygroscopicity and cloud droplet activation of mineral dust aerosol, Geophys. Res. Lett., 36, L08805, doi:10.1029/2009GL037348, 2009.

Kolgotin, A., Korenskiy, M., and Veselovskii, I.: Direct estimation of fine and coarse mode particle parameters from multiwavelength lidar measurements, in: Proceedings of the 27th International Laser Radar Conference, New York City, 5–10 July 2015, SA5.10, 2015.

Kumar, P., Sokolik, I. N., and Nenes, A.: Parameterization of cloud droplet formation for global and regional models: including adsorption activation from insoluble CCN, Atmos. Chem. Phys., 9, 2517-2532, doi:10.5194/acp-9-2517-2009, 2009.

Kumar, P., Sokolik, I. N., and Nenes, A.: Cloud condensation nuclei activity and droplet activation kinetics of wet processed regional dust samples and minerals, Atmos. Chem. Phys., 11, 8661-8676, doi:10.5194/acp-11-8661-2011, 2011.

Liu, J. and Li, Z.: Estimation of cloud condensation nuclei concentration from aerosol optical quantities: influential factors and uncertainties, Atmos. Chem. Phys., 14, 471–483, doi:10.5194/acp-14-471-2014, 2014.

Mamouri, R. E. and Ansmann, A.: Fine and coarse dust separation with polarization lidar, Atmos. Meas. Tech., 7, 3717–3735, doi:10.5194/amt-7-3717-2014, 2014.

Mamouri, R. E. and Ansmann, A.: Estimated desert-dust ice nuclei profiles from polarization lidar: methodology and case studies, Atmos. Chem. Phys., 15, 3463–3477, doi:10.5194/acp-15-3463-2015, 2015.

Mamouri, R. E., Ansmann, A., Nisantzi, A., Kokkalis, P., Schwarz, A., and Hadjimitsis, D.: Low Arabian dust extinction-to-backscatter ratio, Geophys. Res. Lett., 40, 4762–4766, doi:10.1002/grl.50898, 2013.

Mason, R. H., Si, M., Li, J., Chou, C., Dickie, R., Toom-Sauntry, D., Phlker, C., Yakobi-Hancock, J. D., Ladino, L. A., Jones, K., Leaitch, W. R., Schiller, C. L., Abbatt, J. P. D., Huffman, J. A., and Bertram, A. K.: Ice nucleating particles at a coastal marine boundary layer site: correlations with aerosol type and meteorological conditions, Atmos. Chem. Phys., 15, 12547-12566, doi:10.5194/acp-15-12547-2015, 2015.

Mason, R. H., Si, M., Chou, C., Irish, V. E., Dickie, R., Elizondo, P., Wong, R., Brintnell, M., Elsasser, M., Lassar, W. M., Pierce, K. M., Leaitch, W. R., MacDonald, A. M., Platt, A., Toom-Sauntry, D., Sarda-Estve, R., Schiller, C. L., Suski, K. J., Hill, T. C. J., Abbatt, J. P. D., Huffman, J. A., DeMott, P. J., and Bertram, A. K.: Size-resolved measurements of ice-nucleating particles at six locations in North America and one in Europe, Atmos. Chem. Phys., 16, 1637-1651, doi:10.5194/acp-16-1637-2016, 2016.

Mattis, I., Ansmann, A., Althausen, D., Jaenisch, V., Wandinger, U., Müller, D., Arshinov, Y. F., Bobrovnikov, S., Serikov, I. B.: Relative-humidity profiling in the troposphere with a Raman lidar, Appl. Opt., 41, 6451-6462, 2002.

Mattis, I., Ansmann, A., Müller, D., Wandinger, U., and Althausen, D.: Multiyear aerosol observations with dual-wavelength Raman lidar in the framework of EARLINET, J. Geophys. Res., 109, D13203, doi:10.1029/2004JD004600, 2004.

Mattis, I., Müller, D., Ansmann, A., Wandinger, U., Preißler, J., Seifert, P., and Tesche, M.: Ten years of multiwavelength Raman lidar observations of free–tropopsheric aerosol layers over central Europe: geometrical properties and annual cycle, J. Geophys. Res., 113, D20202, doi:10.1029/2007JD009636, 2008.

McCluskey, C. S., DeMott, P. J., Prenni, A. J., Levin, E. J. T., McMeeking, G. R., Sullivan, A. P., Hill, T. C. J., Nakao, S., Carrico, C. M., and Kreidenweis, S. M.: Characteristics of atmospheric ice nucleating particles associated with biomass burning in the US: Prescribed burns and wildfires, J. Geophys. Res. Atmos., 119, 17, 10,458-10,470, doi:10.1002/2014JD021980, 2014.

Müller, D., Mattis, I., Wandinger, U., Ansmann, A., Althausen, A., and Stohl, A.: Raman lidar observations of aged Siberian and Canadian forest fire smoke in the free troposphere over Germany in 2003: microphysical particle characterization, J. Geophys. Res., 110, D17201, doi:10.1029/2004JD005756, 2005.

Müller, D., Ansmann, A., Mattis, I., Tesche, M., Wandinger, U., Althausen, D., and Pisani, G.: Aerosol-type-dependent lidar ratios observed with Raman lidar, J. Geophys. Res., 112, D16202, doi:10.1029/2006JD008292, 2007.

Müller, D., Weinzierl, B., Petzold, A., Kandler, K., Ansmann, A., Müller, T., Tesche, M., Freudenthaler, V., Esselborn, M., Heese, B., Althausen, D., Schladitz, A., Otto, S., and Knippertz, P.: Mineral dust observed with AERONET Sun photometer, Raman lidar, and in situ instruments during SAMUM 2006: Shape–independent particle properties, J. Geophys. Res., 115, D07202, doi:10.1029/2009JD012520, 2010.

Müller, D., Veselovskii, I., Kolgotin, A., Tesche, M., Ansmann, A., and Dubovik, O.: Vertical profiles of pure dust and mixed smoke-dust plumes inferred from inversion of multiwavelength Raman/polarization lidar data and comparison to AERONET retrievals and in situ observations, Appl. Optics, 52, 3178–3202, doi:10.1364/AO.52.003178, 2013.

Müller, D., Hostetler, C. A., Ferrare, R. A., Burton, S. P., Chemyakin, E., Kolgotin, A., Hair, J. W., Cook, A. L., Harper, D. B., Rogers, R. R., Hare, R. W., Cleckner, C. S., Obland, M. D., Tomlinson, J., Berg, L. K., and Schmid, B.: Airborne Multiwavelength High Spectral Resolution Lidar (HSRL-2) observations during TCAP 2012: vertical profiles of optical and microphysical properties of a smoke/urban haze plume over the north-

eastern coast of the US, Atmos. Meas. Tech., 7, 3487–3496, doi:10.5194/amt-7-3487-2014, 2014.

Murray, B. J., O'Sullivan, D., Atkinson, J. D., and Webb, M. E.: Ice nucleation by particles immersed in supercooled cloud droplets, Chem. Soc. Rev., 41, 6519–6554, doi:10.1039/c2cs35200a, 2012.

Nakajima, T., Higurashi, A., Kawamoto, K., and Penner, J. E.: A possible correlation between satellite-derived cloud and aerosol microphysical parameters, Geophys. Res. Lett., 28, 1171–1174, doi:10.1029/2000GL012186, 2001.

Niemand, M., Möhler, O., Vogel, B., Vogel, H., Hoose, C., Connolly, P., Klein, H., Bingemer, H., DeMott, P., Skrotzki, J., and Leisner, T.: Parameterization of immersion freezing on mineral dust particles: an application in a regional scale model, J. Atmos. Sci., 69, 3077–3092, 2012.

Nisantzi, A., Mamouri, R. E., Ansmann, A., and Hadjimitsis, D.: Injection of mineral dust into the free troposphere during fire events observed with polarization lidar at Limassol, Cyprus, Atmos. Chem. Phys., 14, 12155–12165, doi:10.5194/acp-14-12155-2014, 2014.

Nisantzi, A., Mamouri, R. E., Ansmann, A., Schuster, G. L., and Hadjimitsis, D. G.: Middle East versus Saharan dust extinction-to-backscatter ratios, Atmos. Chem. Phys., 15, 7071–7084, doi:10.5194/acp-15-7071-2015, 2015.

O'Dowd, C. D., and de Leeuw, G.: Marine aerosol production: a review of the current knowledge, Phil. Trans. R. Soc. A, 365, 1753-1774; doi:10.1098/rsta.2007.2043, 2007.

Papayannis, A., Amiridis, V., Mona, L., Tsaknakis, G., Balis, D., Bösenberg, J., Chaikovski, A., De Tomasi, F., Grigorov, I., Mattis, I., Mitev, V., Müller, D., Nickovic, S., Pérez, C., Pietruczuk, A., Pisani, G., Ravetta, F., Rizi, V., Sicard, M., Trickl, T., Wiegner, M., Gerding, M., Mamouri, R. E., D'Amico, G., and Pappalardo, G.: Systematic lidar observations of Saharan dust over Europe in the frame of EARLINET (2000–2002), J. Geophys. Res., 113, D10204, doi:10.1029/2007JD009028, 2008.

Pappalardo, G., Amodeo, A., Apituley, A., Comeron, A., Freudenthaler, V., Linné, H., Ansmann, A., Bösenberg, J., D'Amico, G., Mattis, I., Mona, L., Wandinger, U., Amiridis, V., Alados-Arboledas, L., Nicolae, D., and Wiegner, M.: EARLINET: towards an advanced sustainable European aerosol lidar network, Atmos. Meas. Tech., 7, 2389–2409, doi:10.5194/amt-7-2389-2014, 2014.

Prospero, J. M. and Mayol-Bracero, O. L.: Understanding the transport and impact of African dust on the Caribbean Basin, B. Am. Meteorol. Soc., 94, 1329–1337, doi:10.1175/BAMS-D-12-00142.1, 2013.

Pummer, B. G., Budke, C., Augustin-Bauditz, S., Niedermeier, D., Felgitsch, L., Kampf, C. J., Huber, R. G., Liedl, K. R., Loerting, T., Moschen, T., Schauperl, M., Tollinger, M., Morris, C. E., Wex, H., Grothe, H., Pöschl, U., Koop, T., and Fröhlich-Nowoisky, J.: Ice nucleation by water-soluble macromolecules, Atmos. Chem. Phys., 15, 4077–4091, doi:10.5194/acp-15-4077-2015, 2015.

Quinn, P. K., Bates, T. S., Coffman, D. J., and Covert, D. S.: Influence of particle size and chemistry on the cloud nucleating properties of aerosols, Atmos. Chem. Phys., 8, 1029–1042, doi:10.5194/acp-8-1029-2008, 2008.

Richardson, M. S., DeMott, P. J., Kreidenweis, S. M., Cziczo, D. J., Dunlea, E. J., Jimenez, J. L., Thomson, D. S., Lowell, D., Ashbaugh, L., Borys, R. D., Westphal, D. L., Casuccio, G. S., and Lerschet, T. L.: Measurements of heterogeneous ice nuclei in the western United States in springtime and their relation to aerosol characteristics, J. Geophys. Res., 112, D02209, doi:10.1029/2006JD007500, 2007.

Rodríguez, S., Alastuey, A., Alonso-Pérez, S., Querol, X., Cuevas, E., Abreu-Afonso, J., Viana, M., Pérez, N., Pandolfi, M., and de la Rosa, J.: Transport of desert dust mixed with North African industrial pollutants in the subtropical Saharan Air Layer, Atmos. Chem. Phys., 11, 6663-6685, doi:10.5194/acp-11-6663-2011, 2011.

Rose, D., Nowak, A., Achtert, P., Wiedensohler, A., Hu, M., Shao, M., Zhang, Y., Andreae, M. O., and Pöschl, U.: Cloud condensation nuclei in polluted air and biomass burning smoke near the mega-city Guangzhou, China – Part 1: Size-resolved measurements and implications for the modeling of aerosol particle hygroscopicity and CCN activity, Atmos. Chem. Phys., 10, 3365–3383, doi:10.5194/acp-10-3365-2010, 2010.

Sakai, T., Nagai, T., Orikasa, N., Zaizen. Y., Yamashita, K., Mano, Y., and Murakami, M.: Aerosol characterization by dual-wavelength polarization lidar measurements over Kochi, Japan during the warm seasons of 2008 to 2010, J. Meteorol. Soc. Japan, 91, 789-800, doi:10.2151/jmsj.2013-605, 2013.

Schrod, J., Danielczok, A., Weber, D., Ebert, M., Thomson, E. S., and Bingemer, H. G.: Re-evaluating the Frankfurt isothermal static diffusion chamber for ice nucleation, Atmos. Meas. Tech. Discuss., 8, 12525-12557, doi:10.5194/amtd-8-12525-2015, 2015.

Schmidt, J., Ansmann, A., Bühl, J. Baars, H., Wandinger, U., Müller, D., and Malinka, A. V.: Dual-FOV Raman and Doppler lidar stduies of aerosol-cloud interactions: simultaneous profiling of aerosols, warm-cloud properties, and vertical wind, J. Geophys. Res., 119, 5512–5527, doi:10.1002/2013JD020424, 2014.

Seifert, P., Ansmann, A., Mattis, I., Wandinger, U., Tesche, M., Engelmann, R., Müller, D., Pérez, C., and Haustein, K.: Saharan dust and heterogeneous ice formation: eleven years of cloud observations at a central European EARLINET site, J. Geophys. Res., 115, D20201, doi:10.1029/2009JD013222, 2010.

Seifert, P., Kunz, C., Baars, H., Ansmann, A., Bühl, J., Senf, F., Engelmann, R., Althausen, D., and Artaxo, P.: Seasonal variability of heterogeneous ice formation in stratiform clouds over the Amazon Basin, Geophys. Res. Lett., 42, 5587-5593, doi:10.1002/2015GL064068, 2015.

Shinozuka, Y., Clarke, A. D., Nenes, A., Jefferson, A., Wood, R., McNaughton, C. S., Ström, J., Tunved, P., Redemann, J., Thornhill, K. L., Moore, R. H., Lathem, T. L., Lin, J. J., and Yoon, Y. J.: The relationship between cloud condensation nuclei (CCN) concentration and light extinction of dried particles: indications of underlying aerosol processes and implications for satellite-based CCN estimates, Atmos. Chem. Phys., 15, 7585–7604, doi:10.5194/acp-15-7585-2015, 2015.

Shupe, M. D.: A ground-based multisensor cloud phase classifier, Geophys. Res. Lett., 34, L22809, doi:10.1029/2007GL031008, 2007.

Siebert, H., Beals, M., Bethke, J., Bierwirth, E., Conrath, T., Dieckmann, K., Ditas, F., Ehrlich, A., Farrell, D., Hartmann, S., Izaguirre, M. A., Katzwinkel, J., Nuijens, L., Roberts, G., Schäfer, M., Shaw, R. A., Schmeissner, T.,

Serikov, I., Stevens, B., Stratmann, F., Wehner, B., Wendisch, M., Werner, F., and Wex, H.: The fine-scale structure of the trade wind cumuli over Barbados – an introduction to the CARRIBA project, Atmos. Chem. Phys., 13, 10061–10077, doi:10.5194/acp-13-10061-2013, 2013.

Skupin, A., Ansmann, A., Engelmann, R., Baars, H., and Müller, T.: The Spectral Aerosol Extinction Monitoring System (S?MS): setup, observational products, and comparisons, Atmos. Meas. Tech., 7, 701-712, doi:10.5194/amt-7-701-2014, 2014.

Skupin, A., Ansmann, A., Engelmann, R., Seifert, P., and Müller, T.: 1985 Four-year long-path monitoring of ambient aerosol extinction at a central European urban site: dependence on relative humidity, Atmos. Chem. Phys., 16, 1863-1876, doi:10.5194/acp-16-1863-1930 2016, 2016.

Steinke, I., Hoose, C., Möhler, O., Connolly, P., and Leisner, T.: A new temperature- and humidity-dependent surface site density approach for deposition ice nucleation, Atmos. Chem. Phys., 15, 3703–3717, doi:10.5194/acp-15-3703-2015, 2015.

Taylor, J. W., Choularton, T. W., Blyth, A. M., Liu, Z., Bower, K. N., Crosier, J., Gallagher, M. W., Williams, P. I., Dorsey, J. R., Flynn, M. J., Bennett, L. J., Huang, Y., French, J., Korolev, A., and Brown, P. R. A.: Observations of cloud microphysics and ice formation during COPE, Atmos. Chem. Phys., 16, 799-826, doi:10.5194/acp-16-799-2016, 2016a.

Taylor, J. W., Choularton, T. W., Blyth, A. M., Flynn, M. J., Williams, P. I., Young, G., Bower, K. N., Crosier, J., Gallagher, M. W., Dorsey, J. R., Liu, Z., and Rosenberg, P. D.: Aerosol measurements during COPE: composition, size and sources of CCN and IN at the interface between marine and terrestrial influences, Atmos. Chem. Phys. Discuss., doi:10.5194/acp-2016-84, in review, 2016b.

Tesche, M., Ansmann, A., Müller, D., Althausen, D., Engelmann, R., Freudenthaler, V., and Groß, S.: Vertically resolved separation of dust and smoke over Cape Verde using multiwavelength Raman and polarization lidars during Saharan Mineral Dust Experiment 2008, J. Geophys. Res., 114, D13202, doi:10.1029/2009JD011862, 2009.

Tesche, M., Groß, S., Ansmann, A., Müller, D., Althausen, D., Freudenthaler, V., and Esselborn, M.: Profiling of Saharan dust and biomass-burning smoke with multiwavelength polarization Raman lidar at Cape Verde, Tellus B, 63, 649–676, doi:10.1111/j.1600-0889.2011.00548.x, 2011.

Toledano, C., Wiegner, M., Garhammer, M., Seefeldner, M., Gasteiger, J., Müller, D., and Koepke, P.: Spectral aerosol optical depth characterization of desert dust during SAMUM 2006, Tellus B, 61, 216–228, doi:10.1111/j.1600-0889.2008.00382.x, 2009.

Toledano, C., Wiegner, M., Groß, S., Freudenthaler, V., Gasteiger, J., Müller, D., Müller, T., Schladitz, A., Weinzierl, B., Torres, B., and O'Neill, N. T.: Optical properties of aerosol mixtures derived from sun-sky radiometry during SAMUM-2, Tellus B, 63, 635–648, doi:10.1111/j.1600-0889.2011.00573.x, 2011.

Umo, N. S., Murray, B. J., Baeza-Romero, M. T., Jones, J. M., Lea-Langton, A. R., Malkin, T. L., O'Sullivan, D., Neve, L., Plane, J. M. C., and Williams, A.: Ice nucleation by combustion ash particles at conditions relevant to mixed-phase clouds, Atmos. Chem. Phys., 15, 5195–5210, doi:10.5194/acp-15-5195-2015, 2015.

Veselovskii, I., Dubovik, O., Kolgotin, A., Lapyonok, T., Di Girolamo, P., Summa, D., Whiteman, D. N., Mishchenko, M., and Tanr'e, D.: Application of randomly oriented spheroids for retrieval of dust particle parameters from multiwavelength lidar measurements, J. Geophys. Res., 115, D21203, doi:10.1029/2010JD014139, 2010.

Wandinger, U., Mattis, I., Tesche, M., Ansmann, A., Bösenberg, J., Chaikovski, A., Freudenthaler, V., Komguem, L., Linné, H., Matthias, V., Pelon, J., Sauvage, L., Sobolewski, P., Vaughan, G., and Wiegner, M.: Air mass modification over Europe: EARLINET aerosol observations from Wales to Belarus, J. Geophys. Res., 109, D24205, doi:10.1029/2004JD005142, 2004.

Weinzierl, B., Petzold, A., Esselborn, M., Wirth, M., Rasp, K., Kandler, K., Schütz, L., Koepke, P., and Fiebig, M.: Airborne measurements of dust layer properties, particle size distribution and mixing state of Saharan dust during SAMUM 2006, Tellus B, 61, 96–117, doi:10.1111/j.1600-0889.2008.00392.x, 2009.

Wex, H., DeMott, P. J., Tobo, Y., Hartmann, S., Rösch, M., Clauss, T., Tomsche, L., Niedermeier, D., and Stratmann, F.: Kaolinite particles as ice nuclei: learning from the use of different kaolinite samples and different coatings, Atmos. Chem. Phys., 14, 5529–5546, doi:10.5194/acp-14-5529-2014, 2014.

Wiegner, M. and Geiß, A.: Aerosol profiling with the Jenoptik ceilometer CHM15kx, Atmos. Meas. Tech., 5, 1953–1964, doi:10.5194/amt-5-1953-2012, 2012.

Wiegner, M., Madonna, F., Binietoglou, I., Forkel, R., Gasteiger, J., Geiß, A., Pappalardo, G., Schäfer, K., and Thomas, W.: What is the benefit of ceilometers for aerosol remote sensing? An answer from EARLINET, Atmos. Meas. Tech., 7, 1979–1997, doi:10.5194/amt-7-1979-2014, 2014.

Zhang, D., Wang, Z., and Liu, D.: A global view of midlevel liquid-layer topped stratiform cloud distribution and phase partition from CALIPSO and CloudSat measurements, J. Geophys. Res., 115, D00H13, doi:10.1029/2009JD012143, 2010.

Zhang, X., Massoli, P., Quinn, P. K., Bates, T. S., and Cappa, C. D.: Hygroscopic growth of submicron and supermicron aerosols in the marine boundary layer, J. Geophys. Res. Atmos., 119, 83848399, doi:10.1002/2013JD021213, 2014.

Zieger, P., Fierz-Schmidhauser, R., Gysel, M., Strm, J., Henne, S., Yttri, K. E., Baltensperger, U., and Weingartner, E.: Effects of relative humidity on aerosol light scattering in the Arctic, Atmos. Chem. Phys., 10, 3875-3890, doi:10.5194/acp-10-3875-2010, 2010.

Zieger, P., Fierz-Schmidhauser, R., Weingartner, E., and Baltensperger, U.: Effects of relative humidity on aerosol light scattering: results from different European sites, Atmos. Chem. Phys., 13, 10609-10631, doi:10.5194/acp-13-10609-2013, 2013.

Table 1. Available AERONET data sets (individual observational cases) of particle optical and microphysical properties for the three defined basic aerosol types. A total number of 1745 level-2.0 data sets with AOT and column size distributions for Limassol and of 2157 data sets for Leipzig are available for our correlation study. 125 data sets of desert dust optical properties and inverted particle size distributions are selected from the SAMUM and SALTRACE field campaign observations. 123 respective Ragged Point observations (Barbados) for pure marine conditions could be analyzed for our study. CIMH stands for Caribbean Institute for Meteorology and Hydrology.

Site	Observational period	Observations	Dominating aerosol type
Limassol, Cyprus (CUT-TEPAK, 34.7° N, 33.0° E, 25 m a.s.l.)	July 2011–June 2015	421 134	continental aerosol, AE > 1.6 desert dust, AE < 0.5
Leipzig, Germany (TROPOS, 51.4° N, 12.4° E, 125 m a.s.l.)	May 2001–June 2015	974 33	continental aerosol, AE > 1.6 desert dust, AE < 0.5
Ouarzazate, Morocco (SAMUM-1, 30.9° N, 6.9° W, 1150 m a.s.l.)	May–June 2006	32	desert dust
Praia, Cabo Verde (SAMUM-2, 14.9° N, 23.4° W, 70 m a.s.l.)	January 2008	23	desert dust
Barbados (SALTRACE-1, CIMH, 13.1° N, 59.6° W, 110 m a.s.l.)	June–July 2013	20	desert dust
Barbados (SALTRACE-3, Ragged Point, 13.2° N, 59.4° W, 40 m a.s.l.)	June–July 2014	50	desert dust
Barbados (Ragged Point)	August 2007–February 2015	123	marine aerosol

Table 2. Overview of the data analysis from the basic lidar-derived aerosol optical properties (particle backscatter and extinction coefficients, linear depolarization ratio) to the height profiles of CCN-relevant particle and INP number concentrations. Indices p, m, c, d, and nd stand for particle, and marine, non-desert continental, desert, and non-desert particles, respectively. ss indicates the supersaturation level.

Step	Computed parameters	Equation terms
1	Profiles of particle backscatter coefficient and particle linear depolarization ratio	β_{p}, δ_{p}
2	Separation of desert dust and non-desert-dust backscatter coefficients	β_{d}, β_{nd}
3	Conversion to desert dust, marine and continental particle extinction profiles	σ_{d}, σ_{m}, σ_{c}
4	Conversion to particle number and surface area concentrations (aerosol type $i =$ d, m, and c)	$n_{100,\mathrm{d,dry}}$, $n_{50,\mathrm{m,\,dry}}$, $n_{50,\mathrm{c,dry}}$, $n_{250,i,\mathrm{dry}}$, $s_{i,\mathrm{dry}}$
5	Estimation of $n_{\mathrm{CCN},ss}$ from $n_{50,\mathrm{c,dry}}$, $n_{50,\mathrm{m,dry}}$, and $n_{100,\mathrm{d,dry}}$	$n_{\mathrm{CCN},ss,i}$
6	Estimation of n_{INP} from $n_{250,\mathrm{dry}}$ and s_{dry} for each aerosol type i	$n_{\mathrm{INP},i}$

Table 3. Conversion parameters required in the conversion of particle extinction coefficients into particle number and surface area concentrations with Eqs. (1)–(9) in Sect. 3.2. The values are derived from the extended AERONET data analysis and are given for the laser wavelengths of 355 (380 nm), 532, and 1064 nm. $c_{50,\mathrm{d}}$, $c_{60,\mathrm{c}}$, $c_{100,\mathrm{m}}$ (in cm^{-3} for $\sigma_i = 1\,\mathrm{Mm}^{-1}$), and x_i and respective standard deviations (SD) are obtained from the log-log regression analysis presented in Sect. 4. The maximum (positive) SD is given in the table. The mean values and SD of $c_{250,\mathrm{d}}$, $c_{290,\mathrm{c}}$, $c_{500,\mathrm{m}}$ (in $\mathrm{Mm\,cm}^{-3}$) and $c_{\mathrm{s},i}$ (in 10^{-12} $\mathrm{Mm\,m^2\,cm^{-3}}$) are computed from averaging of all individual observations of these conversion factors of a given data set (listed in Table 1). In the case of the Limassol (Cyprus) and Leipzig (Germany) data, all observations with AE (440–870 nm) > 1.6 are interpreted as continental-aerosol-dominated cases, and the observations with AE (440–870 nm) < 0.5 are assumed to be desert-dust-dominated. During SALTRACE-3 the 340 nm channel of the AERONET photometer was not working properly, so that we provide the respective values for 380 nm.

Desert dust	$c_{100,\mathrm{d}}$	x_d	$c_{250,\mathrm{d}}$	$c_{\mathrm{s,d}}$
Cabo Verde, Barbados, 380 nm	5.8 ± 1.7	0.72 ± 0.05	0.19 ± 0.02	1.90 ± 0.25
Cabo Verde, Barbados, 532 nm	6.5 ± 1.8	0.70 ± 0.05	0.20 ± 0.02	1.94 ± 0.26
Cabo Verde, Barbados, 1064 nm	7.5 ± 2.1	0.69 ± 0.05	0.22 ± 0.03	2.21 ± 0.29
Cyprus, dust, 355 nm	8.5 ± 2.0	0.80 ± 0.04	0.16 ± 0.03	2.60 ± 0.55
Cyprus, dust, 532 nm	11.8 ± 2.7	0.76 ± 0.04	0.18 ± 0.03	2.90 ± 0.61
Cyprus, dust, 1064 nm	20.2 ± 4.9	0.69 ± 0.04	0.23 ± 0.05	3.65 ± 0.85
Germany, dust, 355 nm	9.1 ± 5.7	0.79 ± 0.09	0.17 ± 0.03	2.32 ± 0.52
Germany, dust, 532 nm	13.9 ± 8.6	0.73 ± 0.09	0.20 ± 0.03	2.66 ± 0.68
Germany, dust, 1064 nm	20.3 ± 14.0	0.68 ± 0.10	0.23 ± 0.03	3.14 ± 1.02
Continental aerosol	$c_{60,\mathrm{c}}$	x_c	$c_{290,\mathrm{c}}$	$c_{\mathrm{s,c}}/1.33$
Cyprus, 355 nm	105 ± 28	0.67 ± 0.04	0.05 ± 0.02	2.19 ± 0.73
Cyprus, 532 nm	102 ± 26	0.75 ± 0.05	0.09 ± 0.02	3.87 ± 1.23
Cyprus, 1064 nm	460 ± 79	0.59 ± 0.04	0.31 ± 0.10	13.51 ± 5.17
Germany, 355 nm	12.1 ± 1.7	0.97 ± 0.02	0.06 ± 0.03	1.55 ± 0.46
Germany, 532 nm	25.3 ± 3.3	0.94 ± 0.03	0.10 ± 0.04	2.80 ± 0.89
Germany, 1064 nm	108 ± 14	0.85 ± 0.03	0.33 ± 0.16	8.98 ± 3.69
Marine aerosol	$c_{100,\mathrm{m}}$	x_m	$c_{500,\mathrm{m}}$	$c_{\mathrm{s,m}}/4$
Barbados, 355 nm	2.7 ± 1.6	1.06 ± 0.11	0.05 ± 0.01	0.52 ± 0.09
Barbados, 532 nm	7.2 ± 3.7	0.85 ± 0.11	0.06 ± 0.01	0.63 ± 0.11
Barbados, 1064 nm	35.4 ± 12.3	0.50 ± 0.08	0.09 ± 0.02	0.95 ± 0.22

Table 4. Typical uncertainties in the lidar-derived particle optical properties (for 532 nm wavelength), in the retrieved microphysical particle properties, and the estimated cloud-relevant quantities.

Parameter		Relative uncertainty
Backscatter coefficient	β_p	5-10%
Backscatter coefficient (desert dust)	β_d	10-15%
Backscatter coefficient (continental)	β_c	10-20%
Backscatter coefficient (marine)	β_m	20% (PBL)
Extinction coefficient (desert dust)	σ_d	15-25%
Extinction coefficient (continental)	σ_c	20-30%
Extinction coefficient (marine)	σ_m	25% (PBL)
Number concentrations (dry radius >50 nm)	$n_{50,i,\mathrm{dry}}$	Factor of 1.5-2
Number concentrations (dry radius >100 nm)	$n_{100,i,\mathrm{dry}}$	Factor of 1.5-2
Number concentrations (dry radius >250 nm)	$n_{250,i,\mathrm{dry}}$	30-50%
Surface area concentration	$s_{i,\mathrm{dry}}$	30-50%
Number concentration (CCN reservoir)	$n_{\mathrm{CCN},ss,i}$	Factor of 2–3
INP number concentration	$n_{\mathrm{INP},i}$	Factor of 3–10

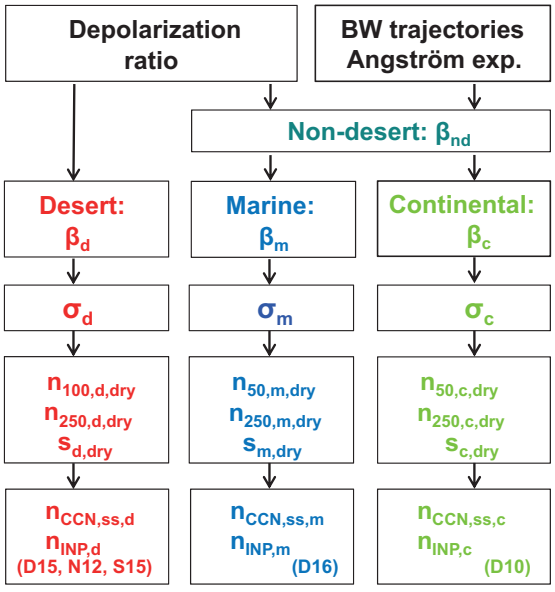

Fig. 1. Overview of the entire data analysis scheme. The polarization lidar enables us to separate desert and non-desert backscatter coefficients $\beta_{\rm d}$ and $\beta_{\rm nd}$ by means of the particle linear depolarization ratio. In the next step, the backscatter coefficients for marine particles $\beta_{\rm m}$ and non-desert continental aerosol mixtures $\beta_{\rm c}$ are separated by means of, e.g., backward (BW) trajectory analysis, Ångström exponent information, and by using marine backscatter estimates (see text). The three backscatter coefficients are then converted to aerosol-type-dependent particle extinction coefficients σ_i, which in turn are converted to profiles of particle number concentrations $n_{100,{\rm d,dry}}$, $n_{50,{\rm m,dry}}$, $n_{50,{\rm c,dry}}$, and $n_{250,i,{\rm dry}}$, and particle surface area concentration $s_{i,{\rm dry}}$. Finally, CCN-relevant particle number concentrations $n_{{\rm CCN},ss,i}$ are estimated for a given supersaturation ss as well as ice-nucleating particle number concentrations $n_{{\rm INP},i}$ by applying INP parameterizations from the literature indicated by D10, D15, D16, N12, and S15 for DeMott et al. (2010, 2015, 2016); Niemand et al. (2012) and Steinke et al. (2015), respectively.

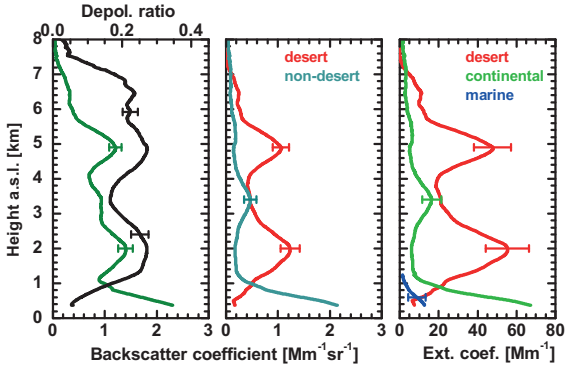

Fig. 2. (Left) 532 nm particle backscatter coefficient (green) and particle linear depolarization ratio (black) as function of height above sea level (a.s.l.), (center) derived particle backscatter coefficients separately for non-desert (marine and continental aerosol, blue-green) and desert particles (red), and (right) particle extinction coefficients separately for marine (blue), continental (green) and desert particles (red). Error bars indicate typical uncertainties. The observation was taken at Nicosia, Cyprus, during a desert dust outbreak from the Sahara on 7 April 2015. Mean profiles for the time period from 20:30–21:30 UTC are shown. The sum of the three extinction profiles match the Raman-lidar-derived total particle extinction profile. Lidar ratios used in the backscatter–to–extinction conversion are 45 sr for desert dust, 35 sr for non-desert continental particles, 20 sr for marine particles in the boundary layer.

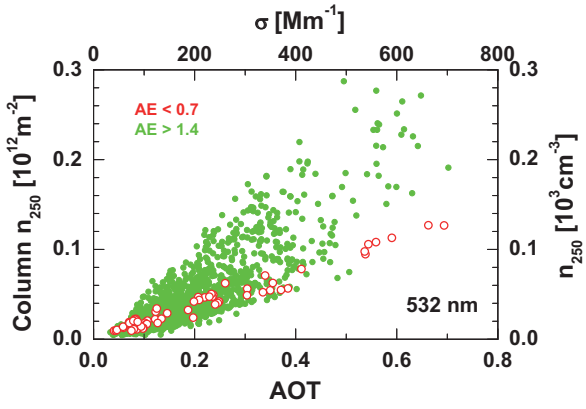

Fig. 3. Replacement of the column integrals (column n_{250}, aerosol optical thickness AOT) obtained from the AERONET observations by volume-related quantities (n_{250}, particle extinction coefficient σ) by assuming an arbitrarily chosen vertical height of the column of 1000 m. In this example, green symbols show all 1523 pollution-dominated Leipzig AERONET observations (2001–2015, level 2.0) with high Ångström exponent (AE > 1.4), and red symbols all 59 dust-dominated cases (AE < 0.7).

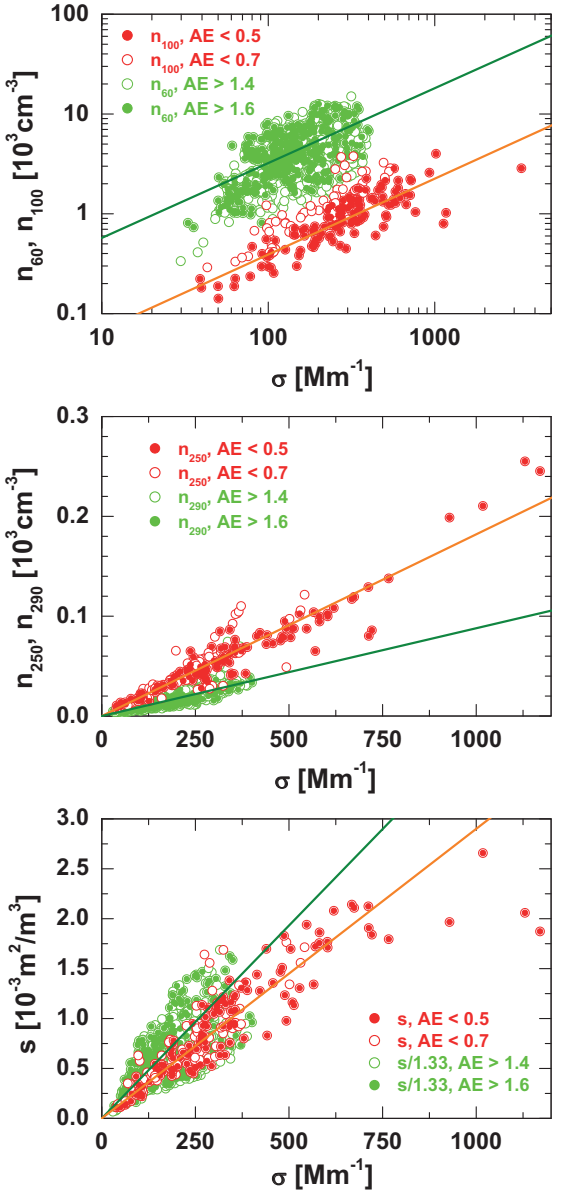

Fig. 4. Particle number concentrations n_{100} (top, red), n_{60} (top, green), n_{250} (center, red), n_{290} (center, green), and particle surface area concentration s (bottom, red) and $s/1.33$ (bottom, green) versus 532 nm particle extinction coefficient σ. AERONET observations (level 2.0) performed at Limassol, Cyprus, from 1 July 2011 to 30 June 2015 are shown. 839, 421, 213, and 134 level-2.0 observations are available at Ångström exponents of AE > 1.4 (open green circles), > 1.6 (solid green circles), < 0.7 (open red circles), and < 0.5 (solid red circles), respectively. The olive lines (for AE > 1.6) and orange lines (for AE < 0.5) indicate the mean increase of $\log n_{100}$ and $\log n_{60}$ with $\log\sigma$ (532 nm, top panel), and the mean increase of n_{250}, n_{290} and s with 532 nm σ.

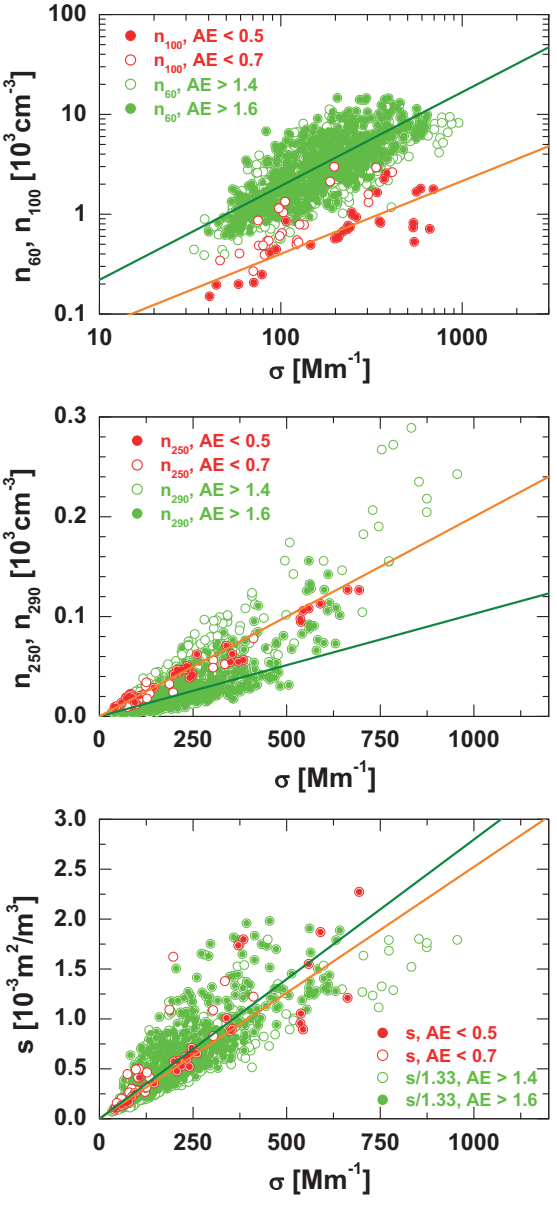

Fig. 5. Same as Fig. 4, except for the AERONET observations at Leipzig from 1 May 2001 and 30 June 2015. 1523, 974, 59, and 33 level-2.0 observations are available at Ångström exponents of AE > 1.4 (open green circles), > 1.6 (solid green circles), < 0.7 (open red circles), and < 0.5 (solid red circles), respectively.

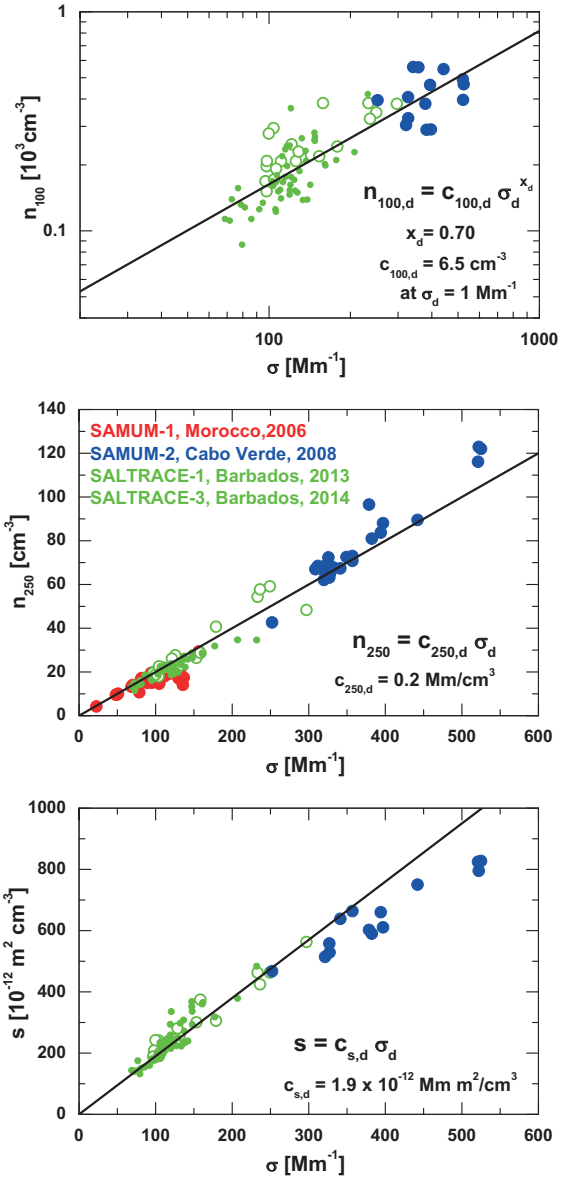

Fig. 6. Relationship between dust layer mean 532 nm extinction coefficient σ and particle number concentrations n_{100} (top) and n_{250} (center), and surface area concentration s (bottom) for observations taken during the desert dust field campaigns in Morocco (red, SAMUM-1, 2006), Cape Verde (blue, SAMUM-2, 2008), and Barbados (open green circles, SALTRACE-1, 2013, solid green circles, SALTRACE-3, 2014). The slope of the black lines are obtained in the same way as in Figs. 4 and 5. Note again, that the n_{250}/σ conversion factor is 0.2 and not 0.67 $\mathrm{Mm\,cm^{-3}}$ as erroneously given in Mamouri and Ansmann (2015).

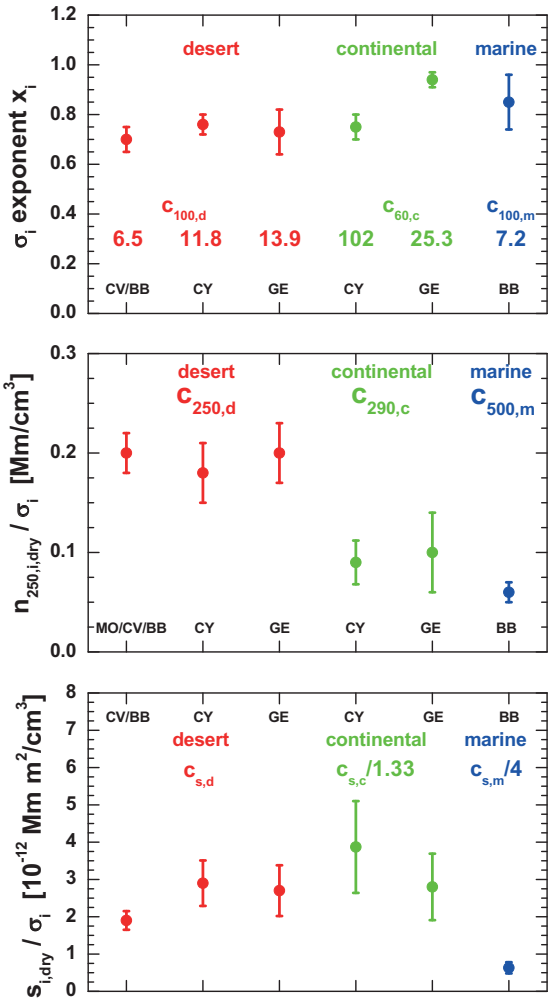

Fig. 7. Overview of derived values for the extinction exponent x_i (top panel, required to compute $n_{100,\mathrm{d,dry}}$, $n_{50,\mathrm{c,dry}}$, and $n_{50,\mathrm{m,dry}}$ with Eqs. 1-3), $c_{250,\mathrm{d}}$, $c_{290,\mathrm{c}}$, and $c_{500,\mathrm{m}}$ (center, required to compute $n_{250,i,\mathrm{dry}}$ with Eqs. 4-6) and $c_{\mathrm{s},i}$ (bottom, required to compute $s_{i,\mathrm{dry}}$ with Eq. 7-9 for 532 nm and the different AERONET data sets listed in Table 3). Values for $c_{100,\mathrm{d}}$, $c_{60,\mathrm{c}}$, and $c_{100,\mathrm{m}}$ (in $\mathrm{cm^{-3}}$ at $\sigma = 1\,\mathrm{Mm^{-1}}$ are required to solve Eq. 1-3) are given as numbers at the bottom of the top panel. Error bars (SD) indicate the uncertainties in the derived parameters. MO, CV, BB indicate SAMUM/SALTRACE dust observations, GE Leipzig, CY Limassol measurements, and BB denotes the Barbados Ragged Point 2007–2015 long-term observations.

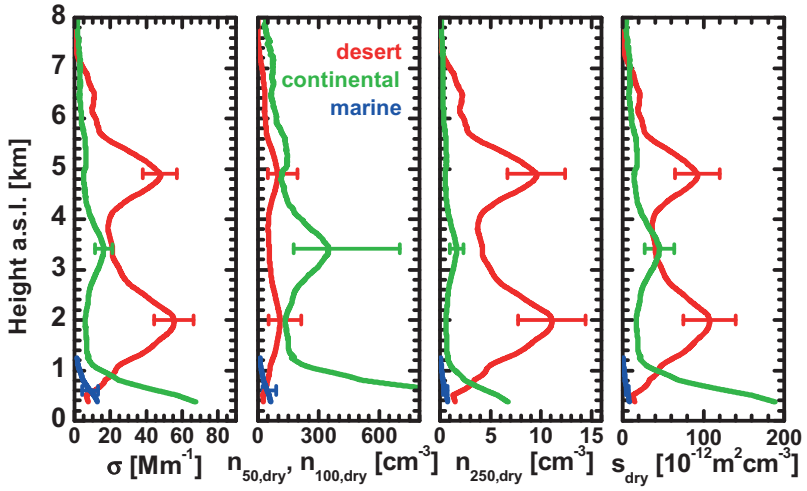

Fig. 8. Height profiles of the 532 nm aerosol extinction coefficient σ (as shown in Fig. 2), and derived profiles of particle number concentrations $n_{50,\mathrm{dry}}$ (marine, continental) and $n_{100,\mathrm{dry}}$ (desert), of the large particle fraction in terms of $n_{250,\mathrm{dry}}$, and surface area concentration s_{dry}, separately for all three aerosol types. The BACCHUS lidar observation was taken with Polly$^{\mathrm{XT}}$ at Nicosia on 7 April 2015 during a major dust outbreak from the Sahara. Error bars show typical overall retrieval uncertainties.

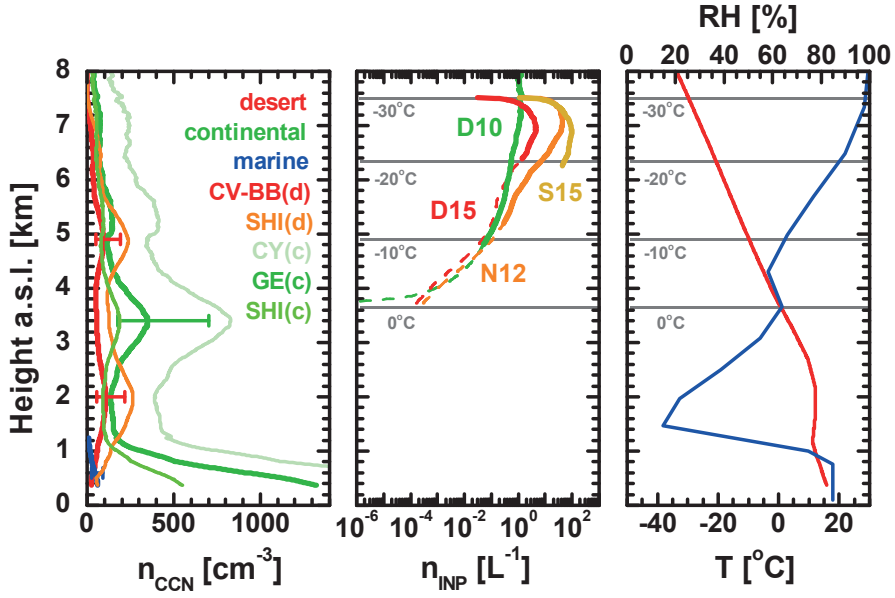

Fig. 9. (Left) Particle number concentration n_{CCN} for a supersaturation of $ss = 0.15\%$ (obtained with Eqs. 10-12). Different parameterizations are used (thick green, GE(c), Germany conversion parameters in Table 3, light green, CY(c), Cyprus parameters, thick red, CV-BB(d), Cabo Verde and Barbados dust conversion parameters, see text for more explanations). In the case of SHI(c) (thin green) and SHI(d) (thin orange) the CCNC parameterization of Shinozuka et al. (2015) is applied. Blue line segment in the PBL shows the estimated marine contribution to CCNC. (Center) Ice-nucleating particle number concentration n_{INP}, computed with the parameterization schemes after DeMott et al. (2010) (D10, Eq. 13), DeMott et al. (2015) (D15, Eq. 14), Niemand et al. (2012) (N12, Eqs. 15-16), and Steinke et al. (2015) (Eqs. 17-19). The respective particle input parameters, $n_{250,\mathrm{d,dry}}$ and $s_{\mathrm{d,dry}}$ are shown in Fig. 8. Solid line segments show the temperature range for which the parameterizations were developed. (Right) GDAS temperature and relative-humidity profiles for Limassol, 7 April 2015, 21 UTC. Error bars (left panel) indicate the estimated uncertainties (factor of 2). n_{INP} errors are estimated to be within a factor of 3-10.

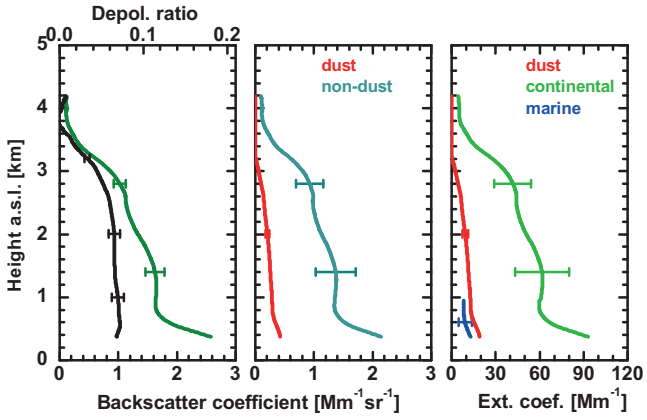

Fig. 10. Same as Fig. 2, except for a lidar observation at Limassol on 16 August 2012. On this day, continental aerosol pollution from Turkey, the Black Sea area, and from southeastern and central Europe was advected to Cyprus at different heights up to 4 km. Lidar ratios used in the conversion of backscatter into extinction profiles were 50–60 sr for continental pollution and 45 sr for mineral dust.

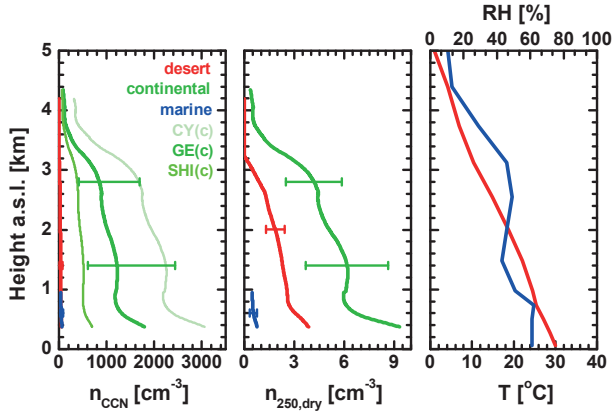

Fig. 11. (Left) Particle number concentration n_{CCN} for a supersaturation of $ss = 0.15\%$. The thick green (GE(c) conversion parameters), red, and blue profiles are obtained with Eqs. (10)-(12) for continental, desert, and marine aerosol, respectively. The thin light green profile (CY(c)) is obtained with Cyprus conversion parameters, and SHI(c) (thin green) with the parameterization of Shinozuka et al. (2015) (see text for more explanations). (Center) Large-particle number concentration $n_{250,\mathrm{dry}}$, computed with Eqs. (4)-(6). (Right) GDAS temperature and relative-humidity profiles for Limassol on 16 August 2012.